PACIFIC EARTHQUAKE ENGINEERING RESEARCH CENTER

Analytical and Experimental Study of Fiber-Reinforced Elastomeric Isolators

James M. Kelly
Shakhzod M. Takhirov
Department of Civil and Environmental Engineering
University of California, Berkeley

PEER 2001/11
SEPTEMBER 2001

Analytical and Experimental Study of Fiber-Reinforced Elastomeric Isolators

James M. Kelly
Professor in the Graduate School
Department of Civil and Environmental Engineering
University of California, Berkeley

and

Shakhzod M. Takhirov
Department of Civil and Environmental Engineering
University of California, Berkeley

PEER Report 2001/11
Pacific Earthquake Engineering Research Center
College of Engineering
University of California, Berkeley

September 2001

ABSTRACT

Theoretical and experimental analyses are carried out for the mechanical characteristics of multi-layer elastomeric isolation bearings where the reinforcing elements, normally steel plates, are replaced by a fiber reinforcement. The fiber-reinforced isolator, in contrast to the steel-reinforced isolator (which is assumed to be rigid both in extension and flexure), is assumed to be flexible in extension, but completely without flexure rigidity.

The influence of fiber flexibility on the mechanical properties of the fiber-reinforced isolator, such as the vertical and horizontal stiffness, is studied, and it is shown that it should be possible to produce a fiber-reinforced isolator that matches the behavior of a steel-reinforced isolator. The fiber-reinforced isolator will be significantly lighter and could lead to a much less labor-intensive manufacturing process.

ACKNOWLEDGMENTS

The sample isolators were handmade by Ahmed Javid of Energy Research, Inc., San Jose, California. The first bearing tests were carried out by Rodney Holland at the Mare Island Test Facility of Applied Structures Technology, LLC. The experimental part of the first step of the research was funded by Energy Research, Inc. The second set of tests was conducted at the Pacific Earthquake Engineering Research Center, University of California, Berkeley. This research work was partly supported by the Engineering Research Center for Met-Shape and Die Manufacturing of Pusan National University, Pusan, Korea, which is gratefully acknowledged.

CONTENTS

LIST OF FIGURES

LIST OF TABLES

1 Introduction

Seismic isolation technology in the United States is applied almost entirely to large, expensive buildings housing sensitive internal equipment, such as computer centers, chip fabrication factories, emergency operation centers, and hospitals. The isolators used in these applications are large, heavy, and expensive. An individual isolator can weigh one ton or more. To extend this effective but expensive earthquake-resistant strategy to housing and commercial buildings, it is necessary to reduce the weight and cost of the isolators.

The primary weight in an isolator is due to the reinforcing steel plates, which are used to provide the vertical stiffness of the rubber-steel composite element. A typical rubber isolator has two large end-plates (around 25 mm thick) and 20 thin reinforcing plates (3 mm thick). The high cost of producing the isolators results from the labor involved in preparing the steel plates and the assembly of the rubber sheets and steel plates for vulcanization bonding in a mold. The steel plates are cut, sand-blasted, acid-cleaned, and then coated with bonding compound. Next, the compounded rubber sheets with the interleaved steel plates are put into a mold and heated under pressure for several hours to complete the manufacturing process. The purpose of the research described in this report is to suggest that both the weight and cost of isolators can be reduced by eliminating the steel reinforcing plates and replacing them with a fiber reinforcement.

The weight reduction is possible because fiber materials are available with an elastic stiffness that is of the same order as steel. Thus the reinforcement needed to provide the vertical stiffness may be obtained by using a similar volume of a much lighter material. The cost savings may be possible if the use of fiber allows a simpler, less labor-intensive manufacturing process. It is also possible that the current approach of vulcanization under pressure in a mold with steam heating can be replaced by microwave heating in an autoclave.

Another benefit to using fiber reinforcement is that it would then be possible to build isolators in long rectangular strips, whereby individual isolators could be cut to the required size. All isolators are currently manufactured as either circular or square in the mistaken belief that if the isolation system for a building is to be isotropic, it needs to be made of symmetrically shaped isolators. Rectangular isolators in the form of long strips would have distinct advantages over square or circular isolators when applied to buildings where the lateral resistance is provided by walls. When isolation is applied to buildings with structural walls, additional wall beams are needed to carry the wall from isolator to isolator. A strip isolator would have a distinct advantage for retrofitting masonry structures and for isolating residential housing constructed from concrete or masonry blocks.

In modeling the isolator reinforced with steel plates, the plates are assumed to be inextensional and rigid in flexure. The fiber reinforcement is made up of many individual fibers grouped in strands and coiled into a cord of sub-millimeter diameter. The cords are more flexible in tension than the individual fibers; therefore, they may stretch when the bearing is loaded by the weight of a building. On the other hand, they are completely flexible in bending, so the assumption made when modeling steel-reinforced isolators—that plane sections remain plane—no longer holds. In fact, when a fiber-reinforced isolator is loaded in shear, a plane cross section becomes curved. This leads to an unexpected advantage in the use of fiber reinforcement. When the bearing is displaced in shear, the tension in the fiber bundle (which acts on the curvature of the reinforcing sheet caused by the shear) produces a frictional damping that is due to individual strands in the fiber bundle slipping against each other. This energy dissipation in the reinforcement adds to that of the elastomer. Recent tests show that this energy dissipation is larger than that of the elastomer. Therefore, when designing a fiber-reinforced isolator for which a specified level of damping is required, it is not necessary to use elaborate compounding to provide the damping because this will be provided by the additional damping from the friction in the fibers.

To calculate the vertical stiffness of a steel-reinforced bearing, an approximate analysis is used that assumes that each individual pad in the bearing deforms in such a way that horizontal planes remain horizontal and points on a vertical line lie on a parabola after loading. The plates are assumed to constrain the displacement at the top and bottom of the pad. Linear elastic behavior with incompressibility is assumed, with the additional assumption that the normal stress components are approximated by the pressure. This leads to the well-known "pressure solution," which is generally accepted as an adequate approximate approach for calculating the vertical stiffness. It is shown that the extensional flexibility of the fiber reinforcement can be incorporated into this approach, and that predictions of the resulting vertical stiffness can be made.

The theoretical analyses have been supplemented by experimental work, and while the tests are only preliminary, they indicate that the concept is viable. The vertical stiffness of the model isolators is in the range of stiffnesses of practical designs of steel-reinforced bearings, with the same diameter (300 mm) and the same thickness of rubber (100 mm). The hysteresis loops generated under combined compression and shear have effective stiffnesses that are somewhat (~20%) less than the equivalent steel-reinforced bearing, but have the same general characteristics and show stable behavior up to a peak shear strain of 150%.

The development of lightweight, low-cost isolators is crucial if this method of seismic protection is to be applied to a wide range of buildings, such as housing, schools, and medical centers, in earthquake-prone areas of the world.

2 Vertical Stiffness of Fiber-Reinforced Bearings

The essential characteristic of the elastomeric isolator is the very large ratio of the vertical stiffness relative to the horizontal stiffness. This is produced by the reinforcing plates, which in current industry standard are thin steel plates. These plates prevent lateral bulging of the rubber, but allow the rubber to shear freely. The vertical stiffness can be several hundred times the horizontal stiffness. The steel reinforcement has a similar effect on the resistance of the isolator to bending moments, usually referred to as the tilting stiffness. This important design quantity makes the isolator stable against large vertical loads.

2.1 Compression of Pad with Rigid Reinforcement

Before developing the solution for flexible reinforcement, it is useful to review the theory for rigid reinforcement. A linear elastic theory is the most common method used to predict the compression and the tilting stiffnesses of a thin elastomeric pad. The first analysis of the compression stiffness was done using an energy approach by Rocard (1937); further developments were made by Gent and Lindley (1959) and Gent and Meinecke (1970). The theory given here is a simplified version of these analyses and is applicable to bearings with shape factors greater than around five.

The analysis is an approximate one based on a number of assumptions. The kinematic assumptions are as follows:

(i) points on a vertical line before deformation lie on a parabola after loading
(ii) horizontal planes remain horizontal

We consider an arbitrarily shaped pad of thickness t and locate a rectangular Cartesian coordinate system, (x, y, z), in the middle surface of the pad, as shown in Fig. 2.1a. Figure 2.1b shows the displacements, (u, v, w) in the coordinate directions under assumptions (i) and (ii):

$$\begin{aligned} u(x, y, z) &= u_0(x, y)\left(1 - \frac{4z^2}{t^2}\right) \\ v(x, y, z) &= v_0(x, y)\left(1 - \frac{4z^2}{t^2}\right) \\ w(x, y, z) &= w(z) \end{aligned} \tag{2.1}$$

This displacement field satisfies the constraint that the top and bottom surfaces of the pad are bonded to rigid substrates. The assumption of incompressibility produces a further constraint on the three components of strain, $\varepsilon_{xx}, \varepsilon_{yy}, \varepsilon_{zz}$, in the form

$$\varepsilon_{xx} + \varepsilon_{yy} + \varepsilon_{zz} = 0 \tag{2.2}$$

and this leads to

$$(u_{0,x} + v_{0,y})\left(1 - \frac{4z^2}{t^2}\right) + w_{,z} = 0$$

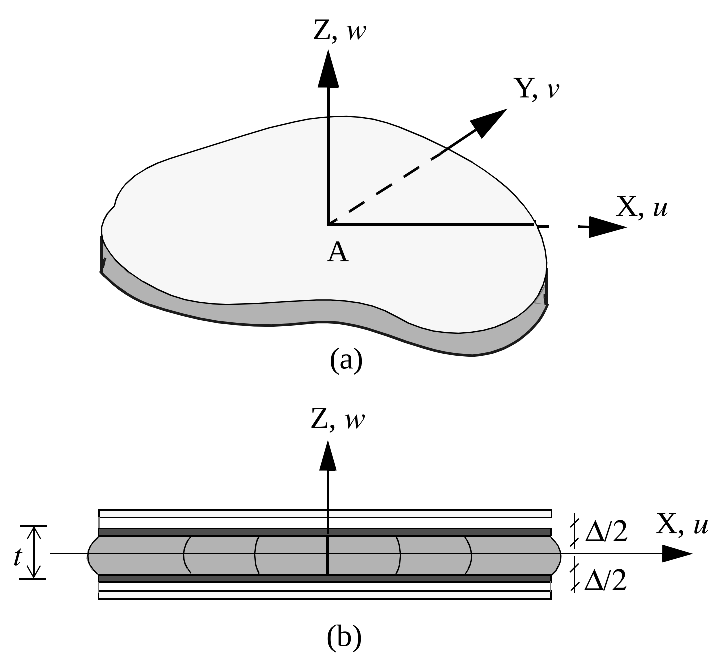

Figure 2.1 Constrained rubber pad and coordinate system

where the commas imply partial differentiation with respect to the indicated coordinate. When integrated through the thickness this gives

$$u_{0,x} + v_{0,y} = \frac{3\Delta}{2t} \tag{2.3}$$

where the change of thickness of the pad is Δ ($\Delta > 0$ in compression).

The stress state is assumed to be dominated by the internal pressure, p, such that the normal stress components, τ_{xx}, τ_{yy}, τ_{zz}, differ from $-p$ only by terms of order $(t^2/l^2)p$, i.e.,

$$\tau_{xx} \approx \tau_{yy} \approx \tau_{zz} \approx -p\left[1 + O\left(\frac{t^2}{l^2}\right)\right]$$

where l is a typical dimension of the pad. The shear stress components, τ_{xz} and τ_{yz}, which are generated by the constraints at the top and bottom of the pad, are assumed to be of order $(t/l)p$; the in-plane shear stress, τ_{xy}, is assumed to be of order $(t^2/l^2)p$.

The equations of equilibrium for the stresses

$$\begin{aligned} \tau_{xx,x} + \tau_{xy,y} + \tau_{xz,z} &= 0 \\ \tau_{xy,x} + \tau_{yy,y} + \tau_{yz,z} &= 0 \\ \tau_{xz,x} + \tau_{yz,y} + \tau_{zz,z} &= 0 \end{aligned}$$

reduce under these assumptions to

$$\begin{aligned} \tau_{xx,x} + \tau_{xz,z} &= 0 \\ \tau_{yy,y} + \tau_{yz,z} &= 0 \end{aligned} \tag{2.4}$$

Assuming that the material is linearly elastic, then shear stresses τ_{xz} and τ_{yz} are related to the shear strains, γ_{xz} and γ_{yz}, by

$$\tau_{xz} = G\gamma_{xz} \quad , \quad \tau_{yz} = G\gamma_{yz}$$

with G being the shear modulus of the material; thus,

$$\tau_{xz} = -8Gu_0\frac{z}{t^2} \quad , \quad \tau_{yz} = -8Gv_0\frac{z}{t^2} \tag{2.5}$$

From the equilibrium equations, therefore,

$$\tau_{xx,x} = \frac{8Gu_0}{t^2} \quad , \quad \tau_{yy,y} = \frac{8Gv_0}{t^2} \tag{2.6}$$

which when inverted to give u_0, v_0 and inserted into the incompressibility condition gives

$$\frac{t^2}{8G}(\tau_{xx,xx} + \tau_{yy,yy}) = \frac{3\Delta}{2t} \tag{2.7}$$

In turn, by identifying both τ_{xx} and τ_{yy} as $-p$, this reduces to

$$p_{,xx} + p_{,yy} = \nabla^2 p = -\frac{12G\Delta}{t^3} = -\frac{12G}{t^2}\varepsilon_c \tag{2.8}$$

where $\varepsilon_c = \Delta/t$ is the compression strain. The boundary condition, $p = 0$, on the perimeter, C, of the pad completes the system for $p(x, y)$.

The vertical stiffness of a rubber bearing is given by the formula

$$K_V = \frac{E_c A}{t_r}$$

where A is the area of the bearing, t_r is the total thickness of rubber in the bearing, and E_c is the instantaneous compression modulus of the rubber-steel composite under the specified level of vertical load. The value of E_c for a single rubber layer is controlled by the shape factor, S, defined as

$$S = \text{loaded area/free area}$$

which is a dimensionless measure of the aspect ratio of the single layer of the elastomer. For example, in an infinite strip of width $2b$, and with a single layer thickness of t, $S = b/t$, and for a circular pad of radius R and thickness t,

$$S = R/2t$$

and for a square pad of side a and thickness t,

$$S = a/(4t)$$

To determine the compression modulus, E_c, we solve for p and integrate over A to determine the resultant normal load, P; E_c is then given by

$$E_c = P/A\varepsilon_c \tag{2.9}$$

where A is the area of the pad.

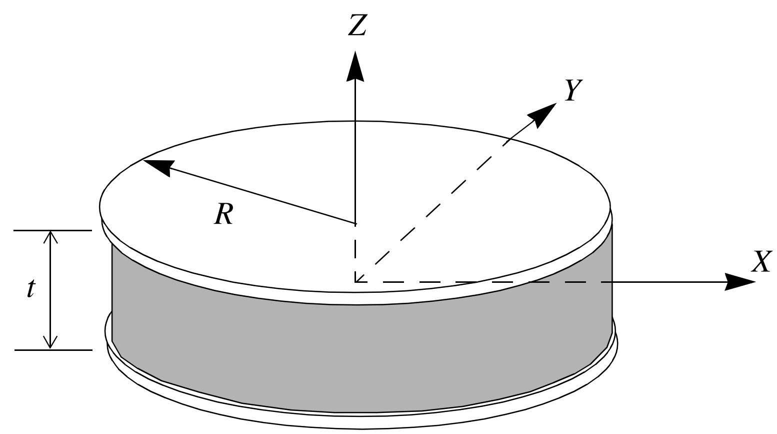

Figure 2.2 Coordinate system for a circular pad of radius *R*

For example, for a circular pad of radius *R*, as shown in Fig. 2.2, Eq. (2.8) reduces to

$$\nabla^2 p = \frac{d^2 p}{dr^2} + \frac{1}{r}\frac{dp}{dr} = -\frac{12G}{t^2}\varepsilon_c; \qquad r = \sqrt{x^2 + y^2}$$

The solution is

$$p = A\ln r + B - \frac{3G}{t^2} r^2 \varepsilon_c$$

where A and B are constants of integration; because p must be bounded at $r = 0$ and $p = 0$ at $r = R$, the solution becomes

$$p = \frac{3G}{t^2}(R^2 - r^2)\varepsilon_c \tag{2.10}$$

It follows that

$$P = 2\pi \int_0^R p(r) r dr = \frac{3G\pi R^4}{2t^2}\varepsilon_c \qquad (2.11)$$

and with $S = \frac{R}{2t}$ and $A = \pi R^2$, we have $E_c = 6GS^2$.

The shear stresses in the rubber exert a shear force on the reinforcing sheet that can be computed from equilibrium, and this shear force, in turn, produces internal tension stresses in the plate. In polar coordinates r, θ, the equations of equilibrium for the stresses in the rubber are, using the notation of Timoshenko (1970),

$$\begin{aligned} \frac{\partial \sigma_r}{\partial r} + \frac{\partial \tau_{rz}}{\partial z} + \frac{\sigma_r - \sigma_\theta}{r} &= 0 \\ \frac{\partial \tau_{rz}}{\partial r} + \frac{\partial \sigma_z}{\partial z} + \frac{\tau_{rz}}{r} &= 0 \end{aligned} \qquad (2.12)$$

We have assumed that $\sigma_r = \sigma_\theta = \sigma_z = -p$, so that from the first

$$\frac{\partial \tau_{rz}}{\partial z} = \frac{\partial p}{\partial r} \qquad (2.13)$$

and with $p = \frac{3G}{t^2}(R^2 - r^2)\varepsilon_c$, then

$$\tau_{rz} = -\frac{6G}{t^2} rz\varepsilon_c \qquad (2.14)$$

The internal forces on the reinforcement are N_r, N_θ, and are caused by the shear stresses, τ_{rz}, on the top and bottom of the shim plate. The internal forces satisfy the equilibrium equation

$$\frac{dN_r}{dr} + \frac{N_r - N_\theta}{r} + \tau_{rz}\big|_{z = -\frac{t}{2}} - \tau_{rz}\big|_{z = -\frac{t}{2}} = 0 \qquad (2.15)$$

or

$$\frac{dN_r}{dr} + \frac{N_r - N_\theta}{r} = \frac{6G}{t} \cdot r \cdot \varepsilon_c$$

If the plate is assumed to be rigid, there is no unique solution of the equilibrium equation; but if we assume it to be deformable, even if the deformations are negligible, we can obtain a unique solution.

The problem is the same as that for the stresses in a thin disk due to centrifugal forces. The solution (Timoshenko 1970) is as follows:

$$\begin{aligned} \sigma_r &= \frac{N_r}{t_f} = \frac{6G}{tt_f} \frac{3+\nu}{8}(R^2 - r^2)\varepsilon_c \\ \sigma_\theta &= \frac{N_\theta}{t_f} = \frac{6G}{tt_f}\left(\frac{3+\nu}{8} R^2 - \frac{1+3\nu}{8} \cdot r^2\right)\varepsilon_c \end{aligned} \tag{2.16}$$

At the center of the plate we have

$$\sigma_{max} = \sigma_r = \sigma_\theta = \frac{6G}{tt_f}\frac{3+\nu}{8}R^2\varepsilon_c \tag{2.17}$$

By expressing the maximum value of the stresses in terms of the average pressure over the plate, p_{ave}, given by

$$p_{ave} = E_c\varepsilon_c = 6GS\varepsilon_c$$

then

$$\frac{\sigma_{max}}{p_{ave}} = \frac{\frac{6G}{tt_f} \cdot \frac{3+\nu}{8}R^2\varepsilon_c}{6GS^2\varepsilon_c} = \frac{3+\nu}{2}\frac{t}{t_f} \tag{2.18}$$

which can be used to determine the maximum pressure needed to cause yield in the shim at the center. It shows why, under normal circumstances, consideration of the stresses in the shims due to the pressure is not considered important. For example, for steel shims 2.5 mm thick and having 13 mm thick rubber layers, the stresses in the steel due to a pressure of 6.90 MPa (which is standard) are only 56.90 MPa.

3 Compression Stiffness with Flexible Reinforcement

The solution for the compression of a pad with rigid reinforcement is algebraically simple enough to be treated in two dimensions and for an arbitrary shape. The problem for the pad with flexible reinforcement is more complicated, however; for simplicity, the derivation will be developed for a circular pad. As before, the rubber is assumed incompressible and the pressure is assumed to be the dominant stress component. The kinematic assumption of quadratically variable displacement is supplemented by an additional displacement that is constant through the thickness and is intended to accommodate the stretching of the reinforcement. Thus

$$\begin{aligned} u_r(r, z) &= u_0(r)\left(1 - \frac{4z^2}{t^2}\right) + u_1(r) \\ w(x, z) &= w(z) \end{aligned} \tag{3.1}$$

The constraint of incompressibility means

$$\varepsilon_r + \varepsilon_\theta + \varepsilon_z = 0$$

where

$$\begin{aligned} \varepsilon_r &= \frac{\partial u_r}{\partial r} = \frac{du_0}{dr}\left(1 - \frac{4z^2}{t^2}\right) + \frac{du_1}{dr} \\ \varepsilon_\theta &= \frac{1}{r}u_r = \frac{1}{r}u_0\left(1 - \frac{4z^2}{t^2}\right) + \frac{1}{r}u_1 \\ \varepsilon_z &= \frac{dw}{dz} \end{aligned} \tag{3.2}$$

leading to

$$\left(\frac{du_0}{dr}+\frac{1}{r}u_0\right)\left(1-\frac{4z^2}{t^2}\right)+\frac{du_1}{dr}+\frac{1}{r}u_1+\frac{dw}{dz} = 0$$

Integration through the thickness with respect to z leads to

$$\left(\frac{du_0}{dr}+\frac{1}{r}u_0\right)+\frac{3}{2}\left(\frac{du_1}{dr}+\frac{1}{r}u_1\right) = \frac{3\Delta}{2t} \tag{3.3}$$

The equations of stress equilibrium in the rubber are

$$\frac{\partial\sigma_r}{\partial r}+\frac{\partial\tau_{rz}}{\partial z}+\frac{\sigma_r-\sigma_\theta}{r} = 0$$
$$\frac{\partial\tau_{rz}}{\partial r}+\frac{\partial\sigma_z}{\partial z}+\frac{\tau_{rz}}{r} = 0$$

Under the basic assumption that the normal stresses, $\sigma_r, \sigma_\theta, \sigma_z$, are all of the same order and approximately equal to the negative of the pressure (i.e., $\sigma_r \approx \sigma_\theta \approx \sigma_z \approx -p$), and that τ_{rz} is one order of magnitude small than p, these reduce to the single equation

$$\frac{\partial\tau_{rz}}{\partial z} = \frac{\partial p}{\partial r} \tag{3.4}$$

The assumption of elastic behavior means that

$$\tau_{rz} = G\gamma_{rz} \tag{3.5}$$

which with

$$\gamma_{rz} = -\frac{8z}{t^2}u_0 \tag{3.6}$$

gives

$$\frac{dp}{dr} = -\frac{8Gu_0}{t^2} \tag{3.7}$$

The internal forces per unit length in the reinforcing sheet are denoted by N_r in the radial direction and N_θ in the tangential direction. If the sheet is made of fiber reinforcement, the individual fibers are replaced by an equivalent sheet of reinforcement of thickness t_f. The internal forces of the equivalent reinforcing sheet are related to the shear stresses on the top and bottom of the pad through the equilibrium equation

$$\frac{dN_r}{dr} + \frac{N_r - N_\theta}{r} - \tau_{rz}\Big|_{z = \frac{t}{2}} + \tau_{rz}\Big|_{z = -\frac{t}{2}} = 0$$

as shown in Fig. 3.1.

From Eqs. (3.5) and (3.6) we have

$$\tau_{rz}\Big|_{z = \frac{t}{2}} = -\frac{8Gu_0}{2t}; \quad \tau_{rz}\Big|_{z = -\frac{t}{2}} = \frac{8Gu_0}{2t}$$

giving

$$\frac{dN_r}{dr} + \frac{N_r - N_\theta}{r} = -\frac{8Gu_0}{t} \tag{3.8}$$

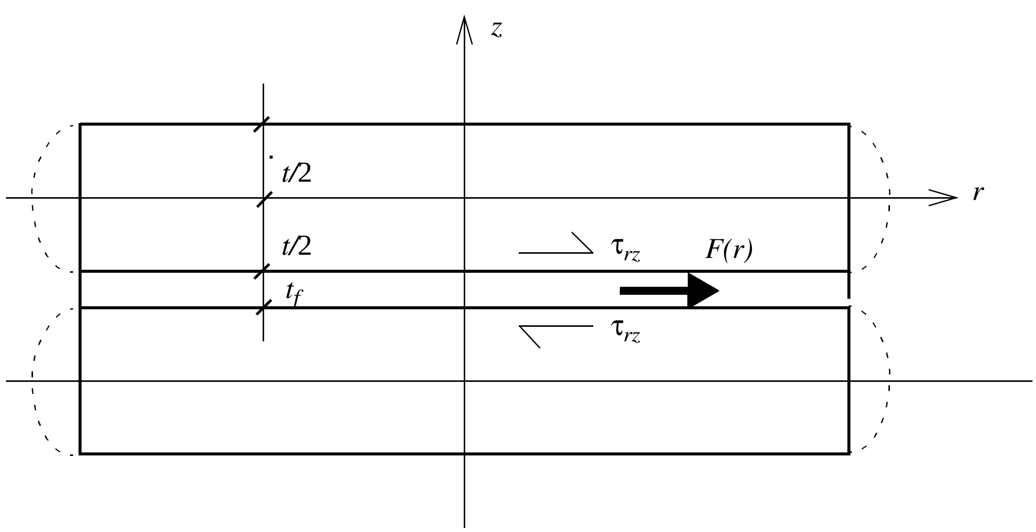

Figure 3.1 Force in equivalent sheet of reinforcement

The extensional strains in the reinforcement, ε_r^f and ε_θ^f, are related to the internal forces through the elastic modulus E_f and Poisson's ratio ν of the equivalent sheet, and its thickness t_f such that

$$\varepsilon_r^f = \frac{N_r - \nu N_\theta}{E_f t_f}; \qquad \varepsilon_\theta^f = \frac{-\nu N_r + N_\theta}{E_f t_f} \tag{3.9}$$

and by inversion

$$\begin{aligned} N_r &= \frac{E_f t_f}{1-\nu^2}(\varepsilon_r^f + \nu\varepsilon_\theta^f) \\ N_\theta &= \frac{E_f t_f}{1-\nu^2}(\nu\,\varepsilon_r^f + \varepsilon_\theta^f) \end{aligned} \tag{3.10}$$

Substitution of these relationships into the equilibrium [Eq. (3.8)] gives

$$\frac{d}{dr}\left[\frac{E_f t_f}{1-\nu^2}\left(\frac{du_1}{dr} + \frac{\nu}{r}u_1\right)\right] + \frac{E_f t_f}{1-\nu^2}\,\frac{(1-\nu)}{r}\left(\frac{du_1}{dr} - \frac{1}{r}u_1\right) + \frac{8Gu_0}{t} = 0$$

Thus

$$u_0 = -\frac{E_f t_f t}{8(1-\nu^2)G}\left[\frac{d^2u_1}{dr^2} + \nu\frac{d}{dr}\left(\frac{u_1}{r}\right) + (1-\nu)\frac{1}{r}\frac{du_1}{dr} - (1-\nu)\frac{u_1}{r^2}\right]$$

which reduces to

$$u_0 = -\frac{E_f t_f t}{8(1-\nu^2)G}\left(\frac{d^2u_1}{dr^2} + \frac{1}{r}\frac{du_1}{dr} - \frac{u_1}{r^2}\right) \tag{3.11}$$

In turn substitution of this into the incompressibility relation [Eq. (3.3)], gives

$$-\frac{E_f t_f t}{8(1-\nu^2)G}\left[\frac{d}{dr}\left(\frac{d^2u_1}{dr^2} + \frac{1}{r}\frac{du_1}{dr} - \frac{u_1}{r^2}\right) + \frac{1}{r}\left(\frac{d^2u_1}{dr^2} + \frac{1}{r}\frac{du_1}{dr} - \frac{u_1}{r}\right)\right] + \frac{3}{2}\left(\frac{du_1}{dr} + \frac{1}{r}u_1\right) = \frac{3}{2}\frac{\Delta}{t}$$

We define a reciprocal length α by

$$\alpha^2 = \frac{12(1-\nu^2)G}{E_f t_f t}$$

leading to

$$\frac{d^3u_1}{dr^3} + \frac{2}{r}\frac{d^2u_1}{dr^2} - \frac{1}{r^2}\frac{du_1}{dr} + \frac{1}{r^3}u_1 - \alpha^2\left(\frac{du_1}{dr} + \frac{u_1}{r}\right) = -\alpha^2\frac{\Delta}{t} \qquad (3.12)$$

The solution of this equation is

$$u_1(r) = C_1 I_1(\alpha r) + BC_2 K_1(\alpha r) + \frac{\Delta}{2t}r + \frac{C_3}{\alpha r} \qquad (3.13)$$

where C_1, C_2, and C_3 are constants of integration, and I_n, K_n are modified Bessel functions of the first and second kind of order n.

By using Eq. (3.7), the relationship between u_0 and u_1 given in Eq. (3.11) can be rewritten as a relationship between p and u_1 in the form

$$\frac{dp}{dr} = \frac{E_f t_f}{(1-\nu^2)t}\left[\frac{d}{dr}\left(\frac{1}{r}\frac{d}{dr}(ru_1)\right)\right]$$

which on integration gives

$$p = -\frac{E_f t_f}{(1-\nu^2)t}\left[\frac{1}{r}\frac{d}{dr}(ru_1) + C_4\right] \qquad (3.14)$$

where C_4 is another constant of integration.

If the pad is annular, $a \le r \le b$, then there are four boundary conditions for the four constants C_1, C_2, C_3, and C_4, namely,

$$N_r(a) = 0 \qquad N_r(b) = 0$$
$$p(a) = 0 \qquad p(b) = 0$$

If the pad is a complete circle of radius R, i.e., $0 \le r \le R$, then $N_r(R) = 0$ and $p(R) = 0$, and boundedness of u_1 and p at $r = 0$. In fact, by the assumption of radial symmetry, $u_1(0) = 0$. Since $K_0(x) \to \ln\frac{2}{x}$ and $K_1(x) \to \frac{1(2)}{x}$ as $x \to 0$, we must have $C_2 = 0$ and $C_3 = 0$.

The remaining constant of integration in Eq. (3.14) must be determined from the requirement that the radial stress in the reinforcement is zero at the edge, $r = R$. From Eq. (3.2) we have

$$\varepsilon_r^f = C_1\alpha\left[I_0(\alpha r) - \frac{1}{\alpha r}I_1(\alpha r)\right] + \frac{1}{2}\frac{\Delta}{t}$$

$$\varepsilon_\theta^f = C_1\alpha\left[\frac{1}{\alpha r}I_1(\alpha r)\right] + \frac{1}{2}\frac{\Delta}{t}$$

Thus

$$N_r(r) = \frac{E_f t_f}{1-\nu^2}\left\{C_1\alpha\left[I_0(\alpha r) - \frac{1-\nu}{\alpha r}I_1(\alpha r)\right] + (1+\nu)\frac{\Delta}{2t}\right\}$$

$$N_\theta(r) = \frac{E_f t_f}{1-\nu^2}\left\{C_1\alpha\left[\nu I_0(\alpha r) + \frac{1-\nu}{\alpha r}I_1(\alpha r)\right] + (1+\nu)\frac{\Delta}{2t}\right\}$$

The requirement that $N_r(R) = 0$ means

$$C_1\alpha = -\frac{1+\nu}{2}\frac{\Delta}{t}\frac{1}{I_0(\alpha R) - \frac{1-\nu}{\alpha R}I_1(\alpha R)} \qquad (3.15)$$

leading to

$$u_1(r) = \frac{\Delta}{2t}\left\{r - \frac{(1+\nu)I_1(\alpha r)}{\alpha\left[I_0(\alpha R) - \frac{1-\nu}{\alpha R}I_1(\alpha R)\right]}\right\} \qquad (3.16)$$

$$N_r(r) = \frac{E_f t_f}{1-\nu^2}\frac{\Delta}{2t}(1+\nu)\left[1 - \frac{I_0(\alpha r) - \frac{1-\nu}{\alpha r}I_1(\alpha r)}{I_0(\alpha R) - \frac{1-\nu}{\alpha R}I_1(\alpha R)}\right] \qquad (3.17)$$

$$N_\theta(r) = \frac{E_f t_f}{1-\nu^2}\frac{\Delta}{2t}(1+\nu)\left[1 - \frac{\nu I_0(\alpha r) + \frac{1-\nu}{\alpha r}I_1(\alpha r)}{I_0(\alpha R) - \frac{1-\nu}{\alpha R}I_1(\alpha R)}\right] \qquad (3.18)$$

The other displacement field needed is $u_0(r)$, which can be obtained by directly substituting Eq. (3.16) into Eq. (3.11). We find that

$$u_0(r) = -\frac{3}{2}C_1 I_1(\alpha r)$$

with C_1 given by Eq. (3.15) above.

To calculate the effective compression modulus, E_c, it is necessary to calculate the pressure distribution, $p(r)$, given by Eq. (3.14). The constant of integration, C_4, can be obtained by the requirement that $p(R) = 0$. The result is

$$p(r) = \frac{12G}{t^2} \cdot \frac{C_1}{\alpha}[I_0(\alpha R) - I_0(\alpha r)] \tag{3.19}$$

The total axial load P is

$$P = 2\pi \int_0^R p(r)\, r dr$$

which with Eq. (3.19) becomes

$$P = 2\pi \frac{12GC_1}{t^2\alpha^3}\left[\frac{1}{2}\alpha^2 R^2 I_0(\alpha R) - \alpha R I_1(\alpha R)\right]$$

which, when C_1 is substituted from Eq. (3.15), becomes

$$P = 2\pi R^2(1+\nu)\frac{E_f t_f}{(1-\nu^2)t} \cdot \frac{\frac{1}{2}\alpha R I_0(\alpha R) - I_1(\alpha r)}{\alpha R I_0(\alpha R) - (1-\nu)I_1(\alpha R)} \frac{\Delta}{t} \tag{3.20}$$

When we equate P with $E_c \varepsilon_c(\pi R^2)$, where

$$\varepsilon_c = \Delta / t$$

is the compression strain, we have

$$E_c = \frac{E_f t_f}{(1-\nu)t} \frac{\frac{1}{2}\alpha R I_0(\alpha R) - I_1(\alpha R)}{\alpha R I_0(\alpha R) - (1-\nu)I_1(\alpha R)} \tag{3.21}$$

By making use of $\alpha^2 = \dfrac{12(1-\nu^2)G}{E_f t_f t}$, this can also be written in the form

$$E_c = \frac{12GR^2}{t^2}(1+\nu)\frac{\frac{1}{2}\alpha R I_0(\alpha R) - I_1(\alpha R)}{\alpha^3 R^3 I_0(\alpha R) - (1-\nu)\alpha^2 R^2 I_1(\alpha R)} \tag{3.22}$$

When the reinforcement stiffness tends to rigidity, then α tends toward zero. Using the power series for I_0 and I_1 we have

$$E_c = \frac{12GR^2}{t^2}(1+\nu)\frac{\frac{\alpha R}{2} + \frac{(\alpha R)^3}{16} + \frac{(\alpha R)^5}{384} - \frac{1}{2}\left[\alpha R + \frac{(\alpha R)^3}{4} + \frac{(\alpha R)^5}{64}\right]}{(\alpha R)^3\left[1 + \frac{(\alpha R)^2}{4}\right] - (1-\nu)\left[\frac{1}{2} + \frac{(\alpha R)^2}{16}\right]} \tag{3.23}$$

$$= 6GS^2\left(1 - \frac{6+\nu}{24(1+\nu)}\alpha^2 R^2\right)$$

The magnitude of the second term in the bracket relative to one is the determining parameter for the importance of the flexibility of the reinforcement. Using the definitions of α^2 and S, this term can be written as

$$\frac{6+\nu}{24(1+\nu)}(\alpha R)^2 = 2(6+\nu)(1-\nu)\cdot\frac{Gt}{E_f t_f}\cdot S^2$$

Thus, for a typical example of a steel shim 2.5 mm thick and a 13 mm rubber layer, with the steel properties $E_f = 207 \times 10^3$ MPa, $\nu = 0.$, and a rubber shear modulus of $G = 1$ MPa and $S = 10$, then $2(6+\nu)(1-\nu)\cdot\dfrac{Gt}{E_f t_f}\cdot S^2 = 0.022$, showing that flexibility is not important.

The compression modulus, E_c, normalized with respect to the compression modulus for rigid reinforcement, $6GS^2$, is plotted in Fig. 3.2 for $\nu = 0$ and $\nu = 1/3$. The figure shows how the modulus decreases with decreasing reinforcement stiffness, E_f, and thickness t_f. The parameter αR can be written in terms of the shape factor, $S = R/(2t)$, as

$$\alpha R = 48(1-\nu^2)\frac{Gt}{E_f t_f}S^2$$

showing that the importance of the flexibility of the reinforcement increases with increasing shape factor (i.e., with thinner layers of elastomer).

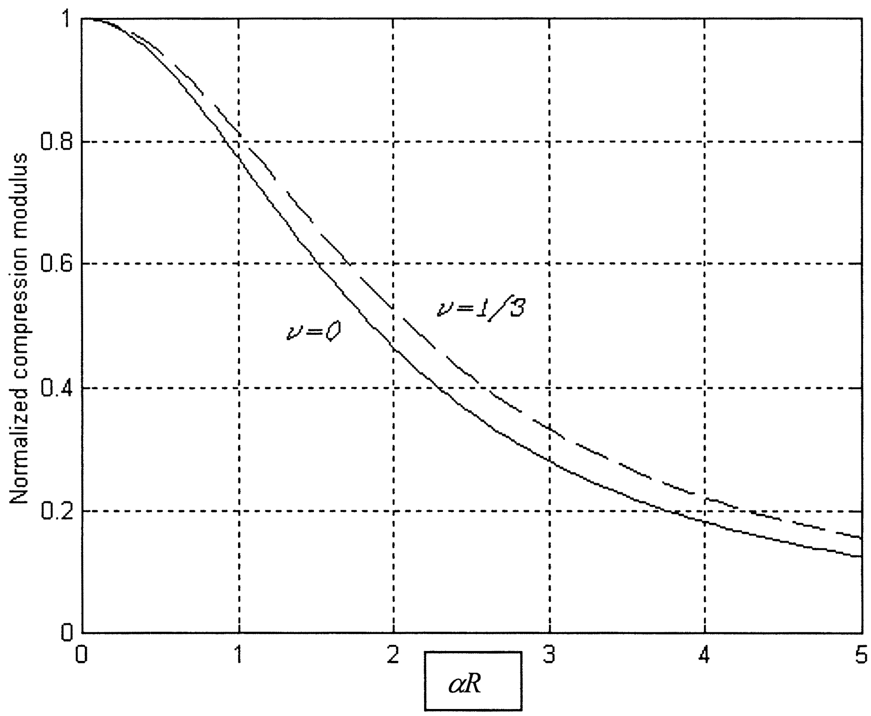

Figure 3.2 Normalized compression modulus $E_c/(6GS^2)$ vs. αR

Returning to the pressure distribution as given by Eq. (3.19) and inserting the value of A from Eq. (3.15), we have

$$p = \frac{6GR^2}{t^2}(1+\nu)\frac{I_0(\alpha R)-I_0(\alpha R)}{\alpha R[\alpha R I_0(\alpha R)-(1-\nu)I_1(\alpha R)]}\varepsilon_c$$

As $E_f \to \infty$, $\alpha \to 0$, we have

$$p = \frac{6GR^2}{t^2}(1+\nu)\frac{\frac{\alpha^4}{4}(R^2-r^2)}{(\alpha R)^2\left[1-\frac{1}{2}(1-\nu)\right]}\varepsilon_c$$

$$= \frac{6GR^2}{t^2}\cdot\frac{1}{2}\left(1-\frac{r^2}{R^2}\right)\varepsilon_c$$

$$= 12GS^2\left(1-\frac{r^2}{R^2}\right)\varepsilon_c$$

If we define the average pressure, p_{ave}, by $p_{ave} = E_c\varepsilon_c$, we have

$$p = 2p_{ave}\left(1-\frac{r^2}{R^2}\right)$$

which is the result [Eq. (2.10)] for rigid reinforcement. It is also possible to show by use of the asymptotic expansions for I_0 and I_1 that as αR tends to infinity, the pressure tends to be uniform with the value $E_c\varepsilon_c$, i.e., $p(r)/p_{ave} \to 1$.

The pressure distribution in the elastomer for various values of αR is shown in Fig. 3.3. The pressure is normalized with respect to the average pressure, $E_c\varepsilon_c$. The effect of the flexibility of the reinforcement is to make the pressure more uniform and to decrease the maximum value.

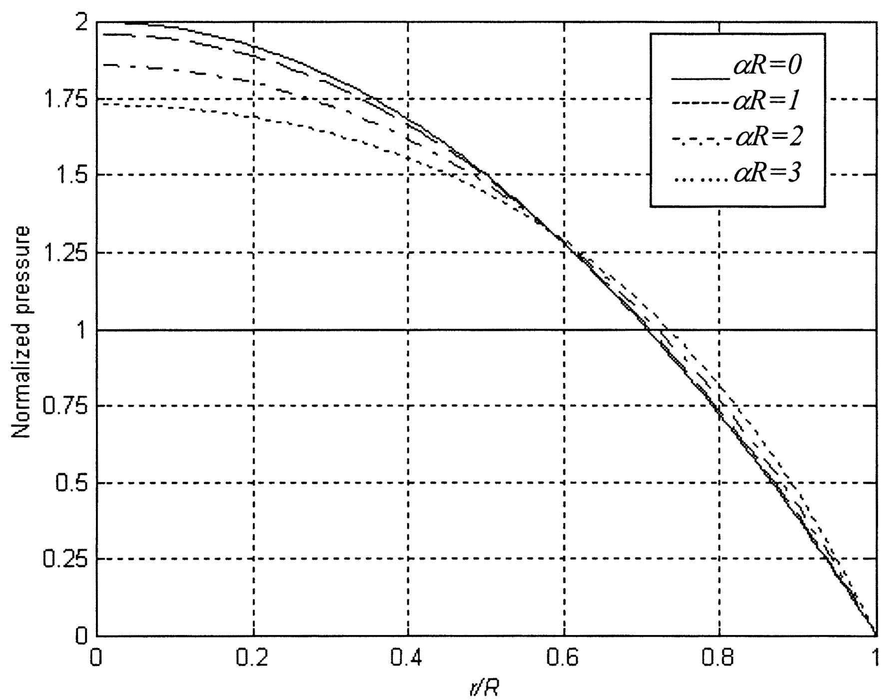

Figure 3.3 Distribution of pressure in pad normalized with respect to average pressure: $p\,/\,(E_c\,\varepsilon_c)$ (solid horizontal line corresponds to $\alpha \to \infty$)

3.1 Stresses in the Reinforcement

The distribution of the in-plane forces in the reinforcement are given by Eqs. (3.17) and (3.18). The quantities N_r and N_θ have units of force per unit length. Dividing them by the reinforcement thickness t_f produces the reinforcement stresses, σ_r^f and σ_θ^f, which can be normalized by dividing by the average pressure, $p_{ave} = E_c \varepsilon_c$. The resulting normalized stresses are proportional to t/t_f, so that it is convenient to show plots of $\sigma_r^f t_f / p_{ave} t$ and $\sigma_r^f t_f / p_{ave} t$ to illustrate the stress behavior.

Using the expressions in Eqs. (3.17) and (3.18) and the expression for E_c given in Eq. (3.21), we have

$$\frac{\sigma_r^f t_f}{p_{ave} t} = \frac{\dfrac{E_f t_f}{(1-\nu)t}\dfrac{\varepsilon_c}{2}\left[1 - \dfrac{I_0(\alpha r) - \dfrac{1-\nu}{\alpha r} I_1(\alpha r)}{I_0(\alpha R) - \dfrac{1-\nu}{\alpha R} I_1(\alpha R)}\right]}{\dfrac{E_f t_f}{2(1-\nu)t}\dfrac{I_0(\alpha R) - \dfrac{2}{\alpha R} I_1(\alpha r)}{I_0(\alpha R) - \dfrac{1-\nu}{\alpha R} I_1(\alpha R)}\varepsilon_c t}$$

$$= \frac{I_0(\alpha R) - \dfrac{1-\nu}{\alpha R} I_1(\alpha r) - I_0(\alpha r) + \dfrac{1-\nu}{\alpha r} I_1(\alpha r)}{I_0(\alpha r) - \dfrac{2}{\alpha r} I_1(\alpha r)}$$

and

$$\frac{\sigma_\theta^f t_f}{p_{ave} t} = \frac{I_0(\alpha R) - \dfrac{1-\nu}{\alpha R} I_1(\alpha R) - \nu I_0(\alpha r) - \dfrac{1-\nu}{\alpha r} I_1(\alpha r)}{I_0(\alpha R) - \dfrac{2}{\alpha R} I_1(\alpha R)}$$

When $r \to 0$, the two stresses are equal and given by

$$\frac{\sigma_r^f(0) t_f}{p_{ave} t} = \frac{I_0(\alpha R) + \left(\dfrac{1-\nu}{\alpha R} I_1(\alpha R)\right) - \dfrac{1+\nu}{2}}{I_0(\alpha R) - \dfrac{2}{\alpha R} I_1(\alpha R)} = \frac{\sigma_\theta^f(0) t_f}{p_{ave} t}$$

These are the largest values and vary from $\frac{3(1+\nu)}{2(1-\nu)}$ when $\alpha R = 0$ to $\frac{(1-\nu)}{2}$ as $\alpha R \to \infty$. At the edge of layer $r = R$, we have, of course, $\sigma_r^f = 0$ and σ_θ^f becomes

$$\frac{\sigma_\theta^f t_f}{p_{ave} t} = (1-\nu)$$

The stress distributions for several values of αR, $\nu = 0$, and $\nu = 1/3$ are shown in Figs. 3.4a and 3.4b and 3.5a and 3.5b.

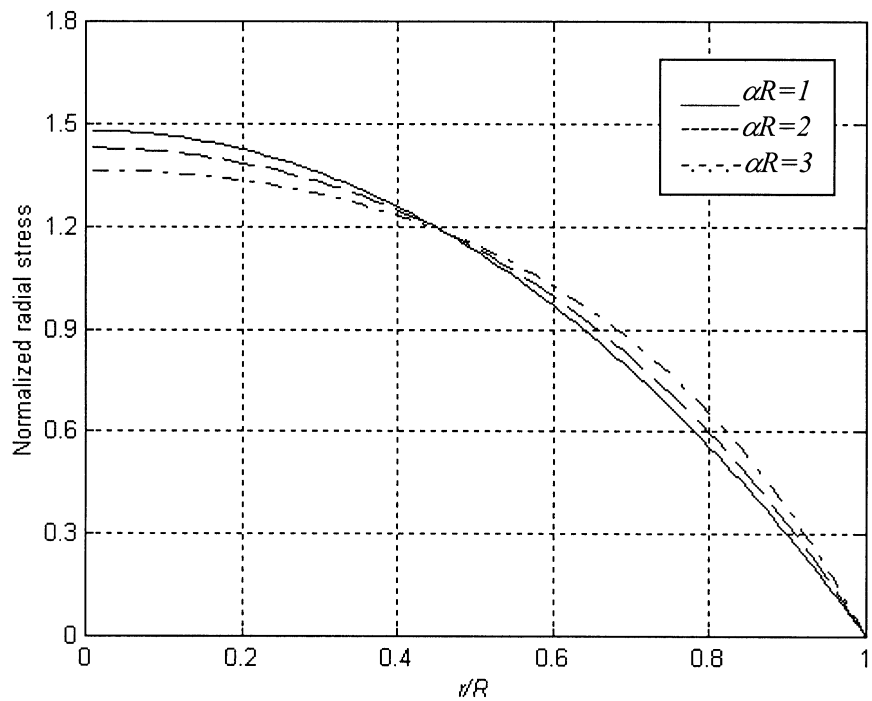

Figure 3.4a Normalized radial stress $\sigma_r^f\, t_f / (p\, t)$ in reinforcement $\nu = 0$

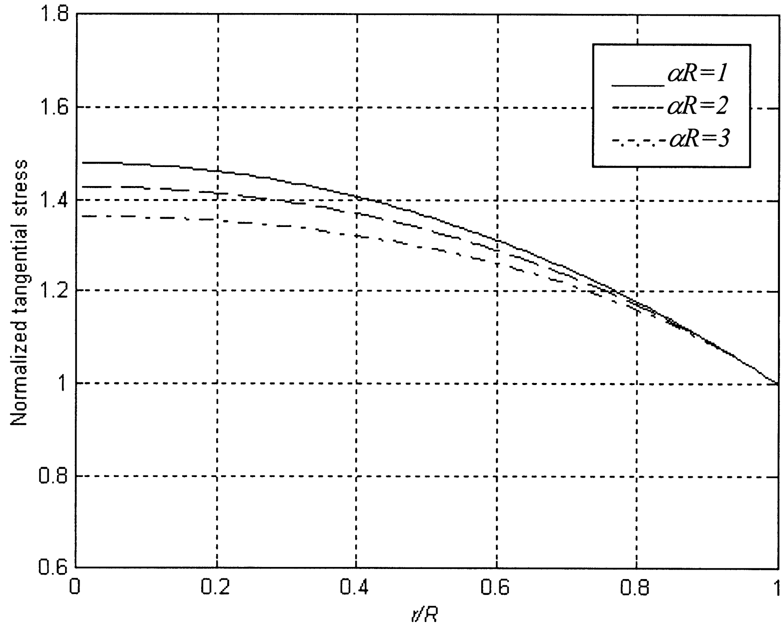

Figure 3.4b Normalized tangential stress $\sigma_\theta^f\, t_f\,/\,(p\ t)$ in reinforcement $\nu = 0$

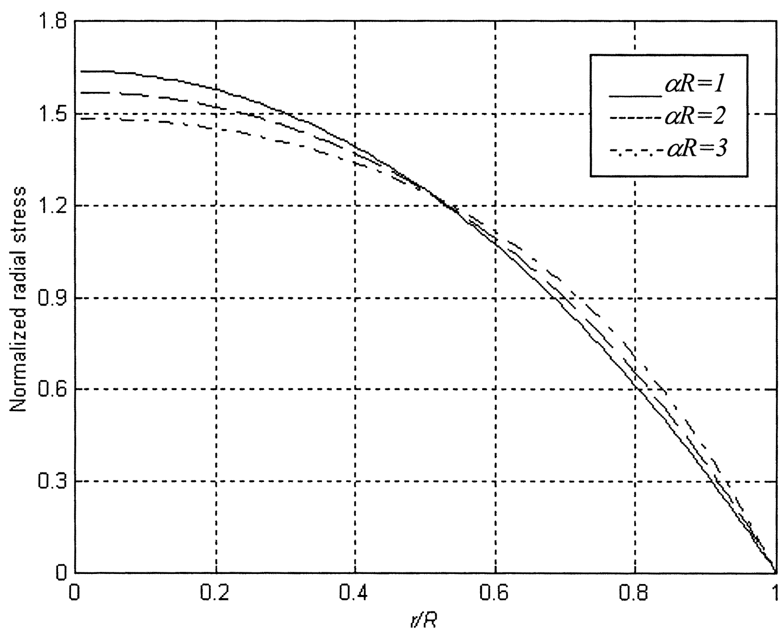

Figure 3.5a Normalized radial stress $\sigma_r^f\, t_f\,/\,(p\ t)$ in reinforcement $\nu = 1/3$

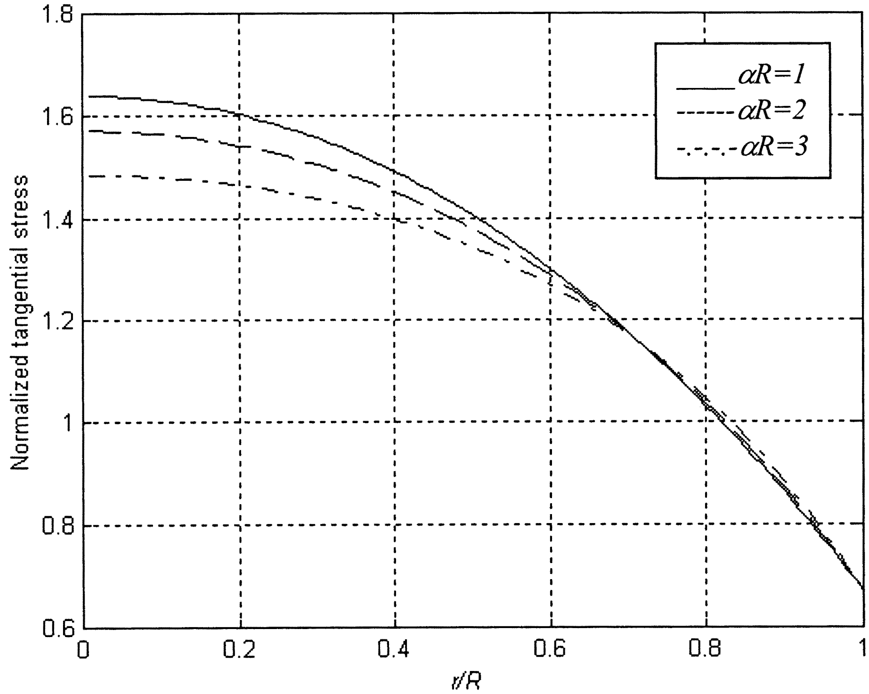

Figure 3.5b Normalized tangential stress $\sigma_\theta^f\, t_f\, /\, (p\ t)$ in reinforcement $\nu = 1/3$

4 Experimental Results

Several samples of fiber-reinforced bearings were constructed and tested in compression to verify if the approach was practical. These bearings were 305 mm in diameter, 140 mm thick, and reinforced by twisted strands of Kevlar. The total thickness of rubber in the bearing was 102 mm. The experimental research was conducted in two stages. During the first stage, the four 305 mm diameter isolators were tested under applied compression. The isolators were tested in shear in pairs (for example, specimen J05 and specimen J06) under a vertical load equivalent to a pressure of 6.90 MPa. The second stage of the experimental study was conducted on only one isolator, specimen J07. The specimen was monotonically loaded up to 6.90 MPa vertical pressure and then three cycles with amplitude ±1.73 MPa were performed. In the final stage the specimen was studied in horizontal shear tests with 6.90 MPa and 3.45 MPa vertical pre-load.

4.1 Performance Parameters of Fiber-Reinforced Bearings

The hysteresis loops obtained during the tests were analyzed to obtain a number of different performance parameters for the fiber-reinforced bearings.

Depending on the loading conditions (axial load and shear strain), the bearing stiffness as revealed by the test hysteresis loops was nonlinear. It is clear that the bearing undergoes a substantial change of stiffness from the small strain to the large strain parts of the test. Two different shear stiffnesses were defined for the test bearings and these were defined for all of the shear tests.

A simple calculation of the effective stiffness based on values of peak force and peak displacement is defined as

$$K^h_{eff} = (F_{max} - F_{min})/(d_{max} - d_{min}) \tag{4.1}$$

Where F_{max}, F_{min}, d_{max}, and d_{min} are the maximum and minimum values of shear force and displacement, respectively. This stiffness is interpreted as the effective or overall stiffness of the bearing during the test.

The other stiffness, K^h_{av}, is defined as the slope of a straight line interpolating the hysteresis loops obtained during cyclic tests. The least squares method was used to calculate this horizontal stiffness and this stiffness is referred to here as the average stiffness of the specimens during cyclic reversals.

The hysteresis loops were also analyzed to obtain the equivalent viscous damping ratio of the bearing for each test. A hysteresis loop represents the plot of force against displacement, and, therefore, the area contained within such a loop represents the energy dissipated by the bearing.

The equivalent viscous damping ratio exhibited by the bearing is evaluated in the usual structural engineering fashion (Clough and Penzien 1975):

$$\xi = W_d /(4\pi W_s) \tag{4.2}$$

where W_d represents a dissipated energy equal to the hysteresis loop area and W_s corresponds to stored or elastic energy defined by the following formula:

$$W_s = (K^h_{eff}\ (\Delta_{max})^2)/2. \tag{4.3}$$

Here, Δ_{max} is the average of the positive and negative maximum displacements and defined as

$$\Delta_{max} = (d_{max} + | d_{min} |)/2. \tag{4.4}$$

The linear viscous model assumes that the energy dissipated in each cycle is linear with the frequency and quadratic with the displacement.

4.2 Experimental Results of the First Series

The force-displacement curves for the three tests at the first stage of the experimental study are shown in Figures 4.1 though 4.3.

The four 305 mm diameter isolators were tested in shear in pairs under a vertical load equivalent to a pressure of 6.90 MPa. They were tested in cyclic shear, with three fully reversed cycles at three maximum strain levels of 50%, 100%, and 150% (based on 102 mm rubber thickness). The results of the tests for one pair (J05/J06) are shown in Figures 4.1 though 4.3.

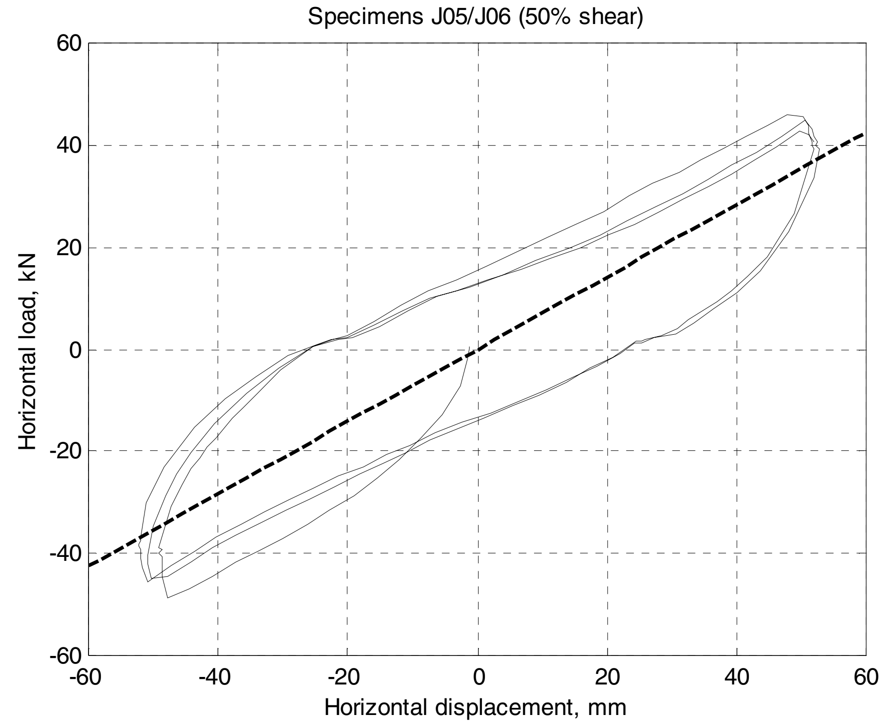

Figure 4.1 Compression-shear test of 305 mm diameter bearings to 50% shear strain

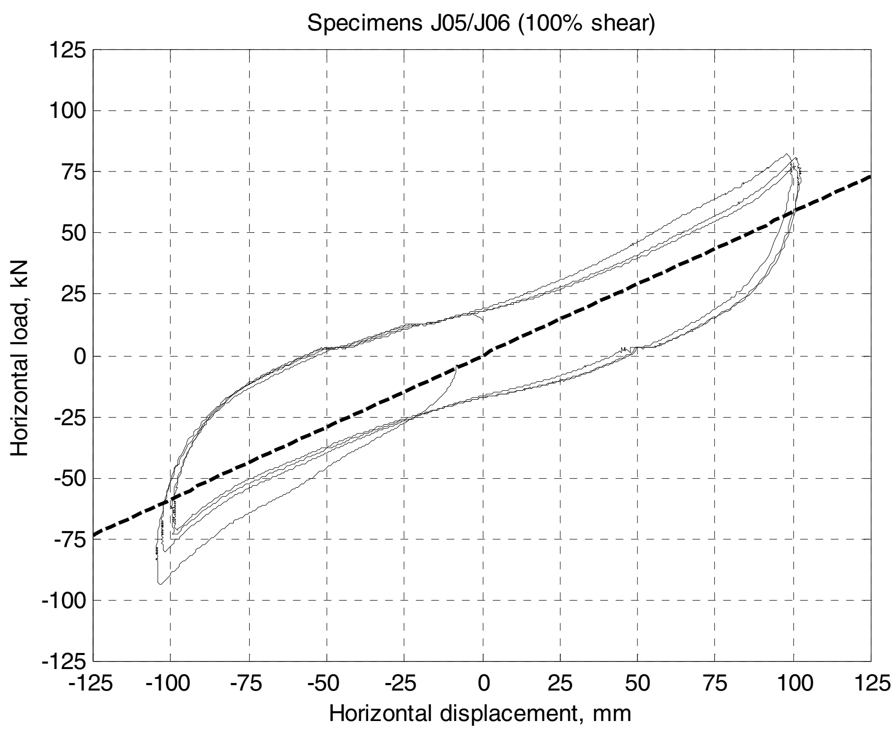

Figure 4.2 Compression-shear test of 305 mm diameter bearings to 100% shear strain

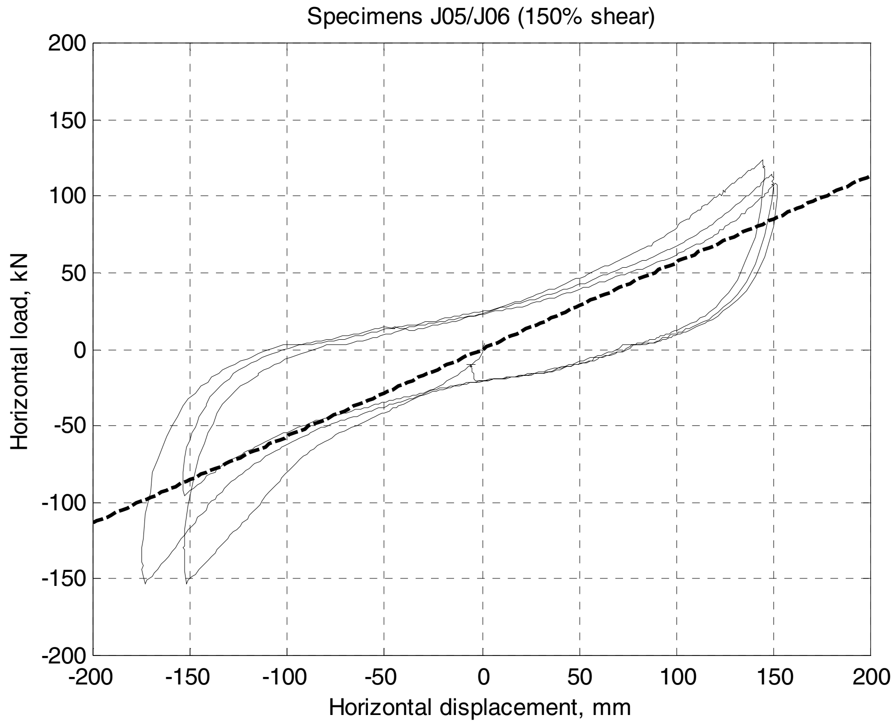

Figure 4.3 Compression-shear test of 305 mm diameter bearings to 150% shear strain (one half-cycle was to 175% shear strain due to operator error)

The dashed straight line corresponds to the horizontal average stiffness of the specimens during the cyclic shear tests. The least squares method was used to calculate this stiffness of the specimens during cyclic reversals. In order to calculate an effective viscous damping ratio of the specimens during the shear tests in the first series, the hysteresis loop of the middle (second) cycle was used.

A short summary of the experimental study on the specimens in the first series is presented in Table 4.1.

Table 4.1 Horizontal test results in the first series (J05 and J06 pair test)

Specimen	Vertical pressure MPa	Shear strain magnitude %	Effective stiffness*, K^h_{eff} kN/m	Average stiffness*, K^h_{av} kN/m	Equivalent damping, ξ %
J05/J06	6.90	50	434	354	17.7
J05/J06	6.90	100	390	293	15.3
J05/J06	6.90	150	345	284	15.5

*The stiffness values represent half of the stiffness calculated for joint shear test of specimens J05 and J06 (the hysteresis loop for the middle cycle was used during calculation).

4.3 Experimental Study during the Second Series

This section summarizes the results of cyclic testing of a fiber-reinforced rubber bearing, namely, specimen J07, which was tested without bonding to the end plates. The tests were carried out in the Structural Research Laboratory of the Pacific Earthquake Engineering Research Center, University of California at Berkeley.

4.3.1 Test Specimen

The photo of the specimen installed in the testing machine is shown in Figure 4.4. It had a cylindrical shape that was 305 mm in diameter with a total height of 140 mm. The total thickness of rubber layers in the bearing was 102 mm.

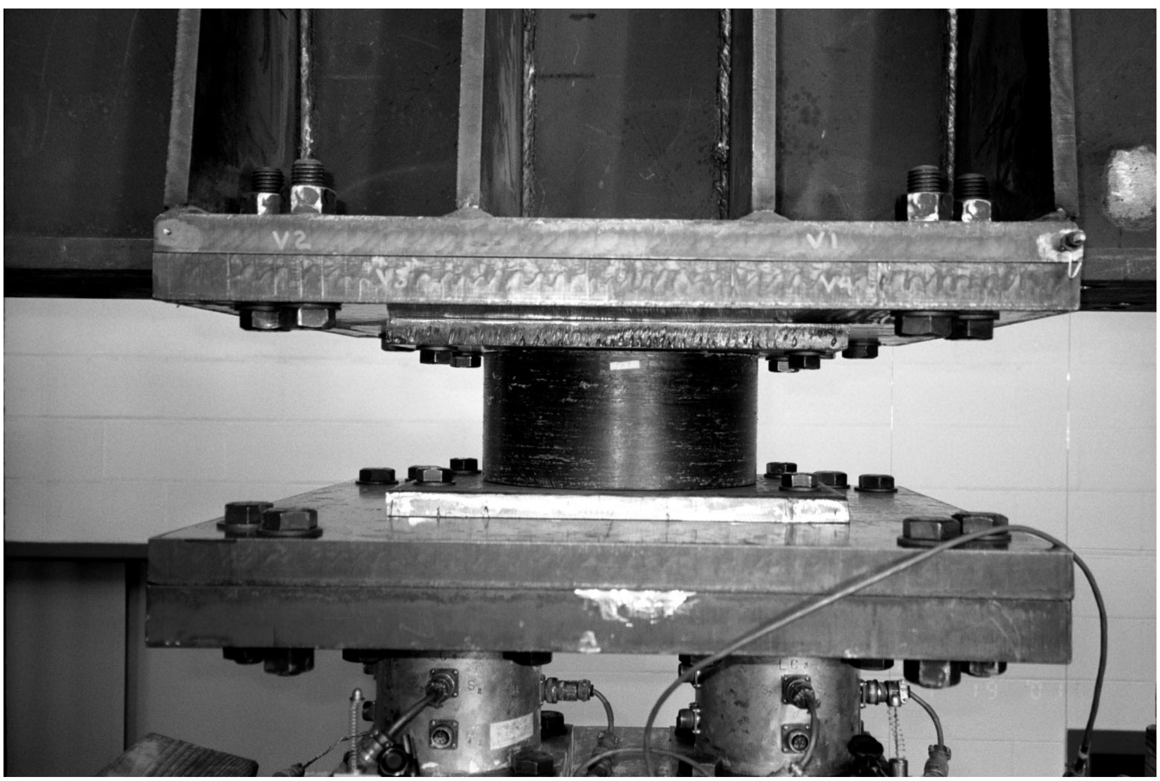

Figure 4.4 Fiber-reinforced rubber bearing installed in the test machine

4.3.2 In-plane Test Machine

The test machine was designed to conduct in-plane vertical and horizontal cyclic loading tests, as shown in Figure 4.5. The vertical load was applied to the specimen by two 570 kN hydraulic actuators, through a stiff frame. The horizontal load was applied to the same frame by a 450 kN hydraulic actuator. The test machine had a displacement capacity of ±254 mm in the horizontal direction and a load capacity of ±1,140 kN in the vertical direction. Two sets of tests were conducted. The vertical test was conducted using a vertical load control, and the horizontal test was performed using a horizontal displacement control. The photograph in Figure 4.6 shows a global view of a test in progress.

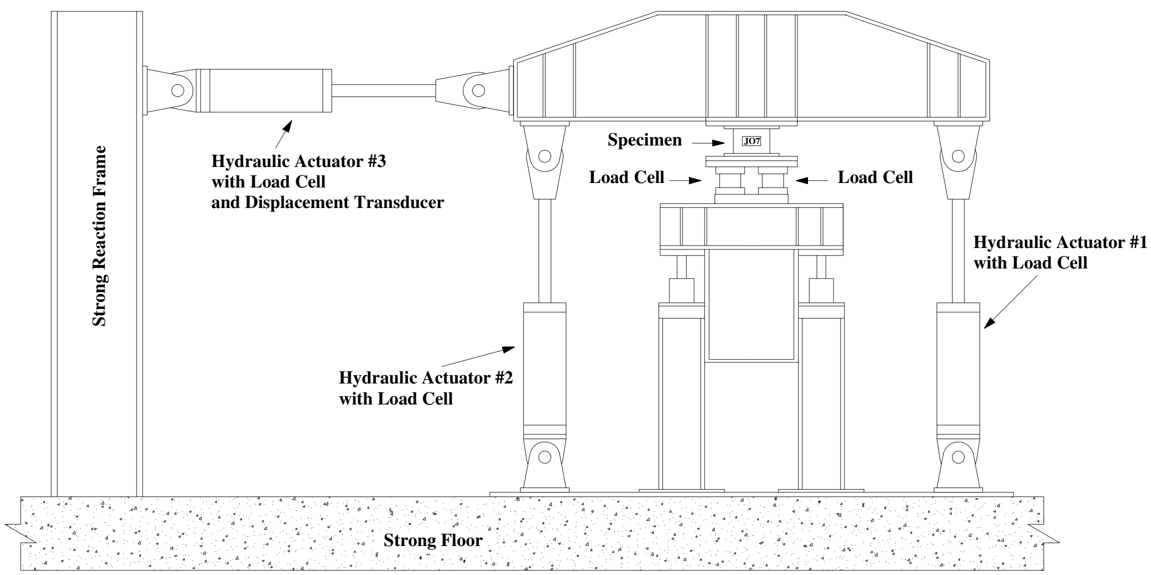

Figure 4.5 Testing setup

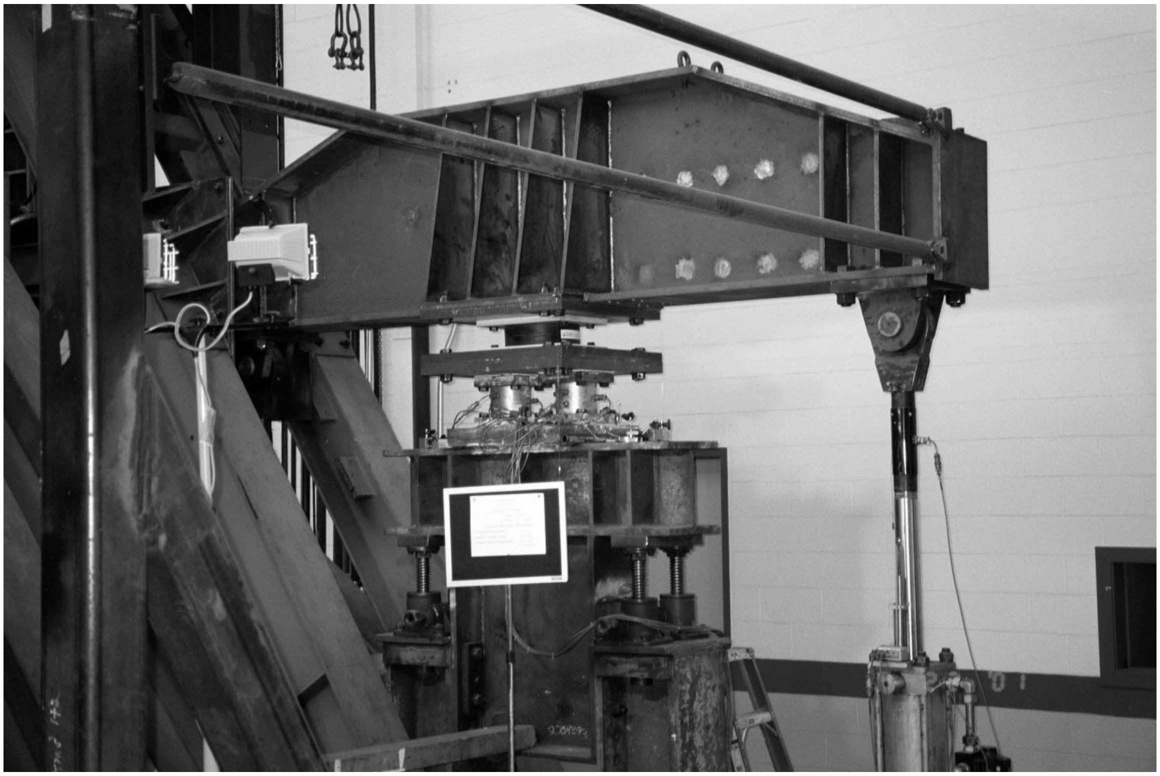

Figure 4.6 Test in progress

4.3.3 Instrumentation

Many sensors were used to monitor the response of the specimen during the test in order to understand the specimen behavior. The instrumentation allocation was slightly different for the vertical and horizontal tests. Tables 4.2 and 4.3 present information on the instrumentation, with the channel number, name of the measuring device, and device location.

Table 4.2. Instrumentation setup for vertical test

Channel No.	Device	Measuring Response	Location	Notations
0	LVDT	Horizontal displacement	Horizontal actuator #3	$\boldsymbol{\delta}$
1	LC	Horizontal load	Horizontal actuator #3	$\boldsymbol{H}$
2	LC	Vertical load	Vertical actuator #1	$\boldsymbol{V_1}$
3	LC	Vertical load	Vertical actuator #2	$\boldsymbol{V_2}$
4	WP	Vertical displacement	Vertical actuator #1	
5	WP	Vertical displacement	Vertical actuator #2	
6	DCDT	Vertical displacement	Vertical actuator #1	
7	DCDT	Vertical displacement	Vertical actuator #2	
8	LC	Shear force	Load cell on support frame (left)	$\boldsymbol{S_1}$
9	LC	Shear force	Load cell on support frame (right)	$\boldsymbol{S_2}$
10	LC	Axial load	Load cell on support frame (left)	$\boldsymbol{A_1}$
11	LC	Axial load	Load cell on support frame (right)	$\boldsymbol{A_2}$
12	DCDT	Vertical displacement	Between isolator’s base plates	$\boldsymbol{\delta_1}$
13	DCDT	Vertical displacement	Between isolator’s base plates	$\boldsymbol{\delta_2}$
14	DCDT	Vertical displacement	Between isolator’s base plates	$\boldsymbol{\delta_3}$
15	DCDT	Vertical displacement	Between isolator’s base plates	$\boldsymbol{\delta_4}$

Table 4.3. Instrumentation setup for horizontal test

Channel No.	Device	Measuring Response	Location	Notations
0	LVDT	Horizontal displacement	Horizontal actuator #3	$\boldsymbol{\delta}$
1	LC	Horizontal load	Horizontal actuator #3	$\boldsymbol{H}$
2	LC	Vertical load	Vertical actuator #1	$\boldsymbol{V_1}$
3	LC	Vertical load	Vertical actuator #2	$\boldsymbol{V_2}$
4	WP	Vertical displacement	Vertical actuator #1	
5	WP	Vertical displacement	Vertical actuator #2	
6	DCDT	Vertical displacement	Vertical actuator #1	
7	DCDT	Vertical displacement	Vertical actuator #2	
8	LC	Shear force	Load cell on support frame (left)	$\boldsymbol{S_1}$
9	LC	Shear force	Load cell on support frame (right)	$\boldsymbol{S_2}$
10	LC	Axial load	Load cell on support frame (left)	$\boldsymbol{A_1}$
11	LC	Axial load	Load cell on support frame (right)	$\boldsymbol{A_2}$
12	DCDT	Vertical displacement	Support frame flexibility	$\boldsymbol{\delta_8}$
13	WP	Vertical displacement	Backup	$\boldsymbol{\delta_7}$
14	DCDT	Vertical displacement	Used in out-of-plane rotation calc.	$\boldsymbol{\delta_6}$
15	DCDT	Vertical displacement	Used in out-of-plane rotation calc.	$\boldsymbol{\delta_5}$

Figure 4.7 shows the location of displacement and load measuring instruments for the vertical testing setup. The imposed vertical loads were measured by load cells built into hydraulic actuators #1 and #2 (V_1 and V_2). The vertical displacement between the base plates of the specimen was averaged from the data of four DCDTs (δ_1 , δ_2 , δ_3 and δ_4) located at four different corners of the bearing base-plates. The horizontal displacement was measured by an LVDT (Linear Variable Differential Transformer) built into hydraulic actuator #3. This displacement is denoted by δ_5 and a load cell in-line with the actuator measured the axial horizontal force H. The shear (S_1 , S_2) and axial loads (A_1, A_2) were measured by two load cells located under the test specimen. The vertical displacement of the top moving frame was measured at two vertical actuator locations.

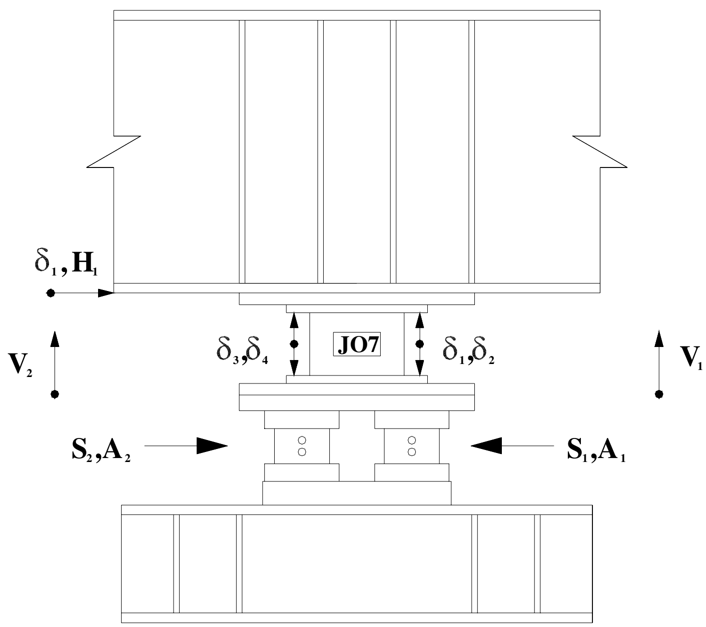

Figure 4.7 Instrumentation setup for vertical test

The instrumentation for the horizontal test is presented in Figure 4.8 with the channel description in Table 4.3, and differs from the previous one. Four channels for measuring the vertical displacement between base plates were exchanged in the following way. Two DCDTs were assigned to measure out-of-plane rotation of the top loading frame (δ_5 and δ_6). One channel was used to measure the horizontal displacement of this frame as a backup channel, δ_7 . One DCDT was used to measure the horizontal flexibility of the bottom support frame, δ_8 .

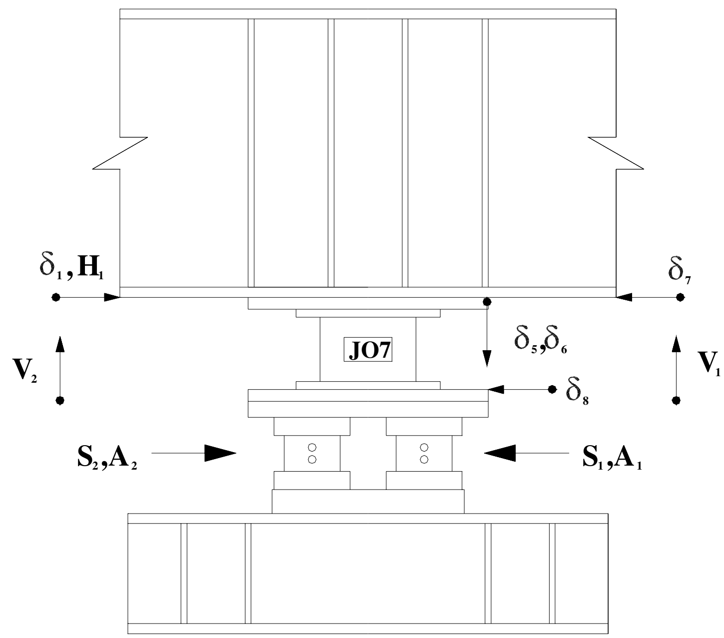

Figure 4.8 Instrumentation setup for horizontal test

4.3.4 Data Acquisition

The test control and the data acquisition system were run by a PC Windows-based control and acquisition program called Automated Testing System (ATS) developed by SHRP Equipment Corporation of Walnut Creek, California. This program is capable of signal generation, four-channel servo-actuator command, and 16-channel data acquisition. The ATS system was used to monitor and control the displacement and force-feedback signals during the tests.

4.3.5 Loading History

The specimen was tested under vertical load control during the vertical test. The specimen was monotonically loaded up to 6.90 MPa vertical pressure, and three fully reversed cycles with amplitude ±1.73 MPa were performed. In the final stage the specimen was monotonically unloaded. The loading history of the vertical test is presented in Figure 4.9.

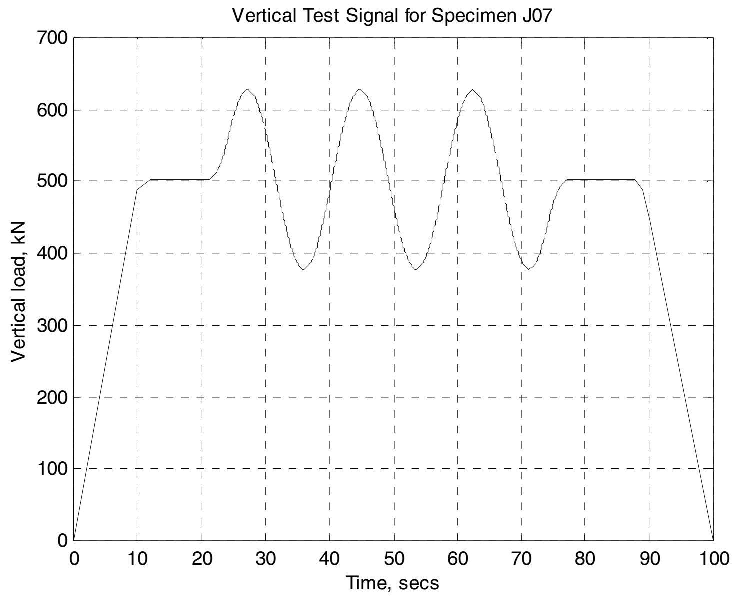

Figure 4.9 Imposed load in vertical testing program

The horizontal test was performed under horizontal displacement control. The specimen was tested in cyclic shear, with three fully reversed cycles at three maximum strain levels of 50%, 100%, and 150% (based on 102 mm rubber thickness). The loading history of the horizontal test is presented in Figure 4.10. These cycles were applied at two values of the equivalent vertical pressure: 6.90 MPa and 3.45 Mpa.

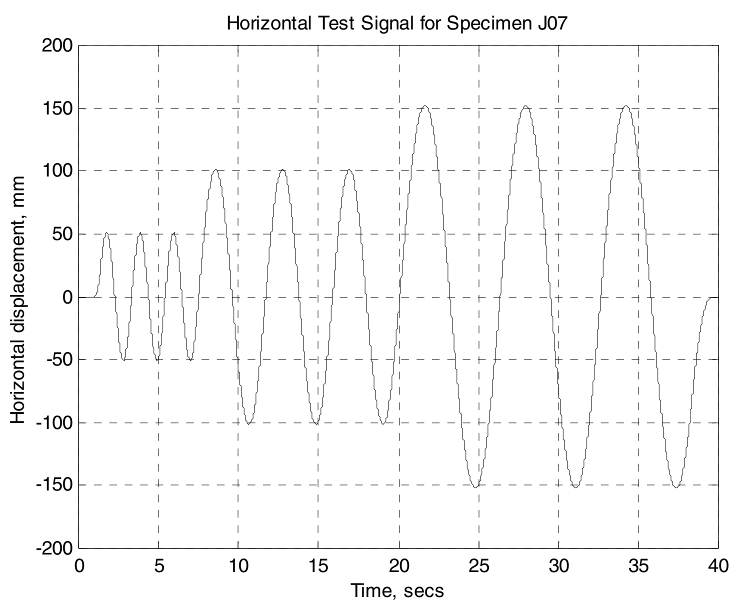

Figure 4.10 Imposed displacement in horizontal test program

Table 4.4 presents the testing program for the specimen in the vertical and horizontal tests.

Table 4.4 Test program for specimen J07

No	Type of testing	Vertical pressure* MPa	Number of cycles	Cycle magnitude	Shear strain magnitude
1	Vertical test	6.90	3	1.73 MPa	N/A
2	Horizontal test	6.90	3	51 mm	50 %
		6.90	3	102 mm	100 %
		6.90	3	153 mm	150 %
3	Horizontal test	3.45	3	51 mm	50 %
		3.45	3	102 mm	100 %
		3.45	3	153 mm	150 %

* The vertical load was monotonically applied from 0 to target value; the vertical pressure represents average pressure on the top of the bearing at the target value.

4.3.6 Data Processing

The specimen behavior was characterized by the following parameters during the vertical test: applied load and vertical displacement between top and bottom end plates. The applied vertical load was averaged from the two load cells located under the specimen (A_1, A_2). The relative vertical displacement between the end plates of the specimen was averaged from four DCDT data (δ_1, δ_2, δ_3 and δ_4) that were located at the four corners of the end plates.

During the horizontal test the specimen behavior was characterized by the applied horizontal load and the horizontal displacement of the top frame. The imposed horizontal load was computed as a sum of two shear loads measured by two load cells located under the test specimen (S_1, S_2). The relative horizontal displacement of the top loading frame was obtained from the horizontal displacement (δ_7) of the frame minus the horizontal displacement of the loading table (δ_8).

The least squares method was used to calculate the average stiffness of the specimen during cyclic reversals. The average stiffness was calculated for the vertical and horizontal directions. For both directions the data from the corresponding cyclic test were used. In order to calculate an effective viscous damping ratio of the specimen during the shear tests with different vertical pre-load, the hysteresis loops of three cycles with the same shear deformation magnitude were used.

A set of programs for the MATLAB 5.3 environment was created to process the data and to plot results in accordance with the procedure described above.

4.3.7 Test Results

The specimen was tested on January 19, 2001. The specimen sustained all loading steps up to and including the 150% shear deformation cycles with no damage. Figures 4.11–4.13, respectively, show the specimen under 50%, 100%, and 150% shear deformation during the horizontal tests with vertical pressure of 6.90 MPa.

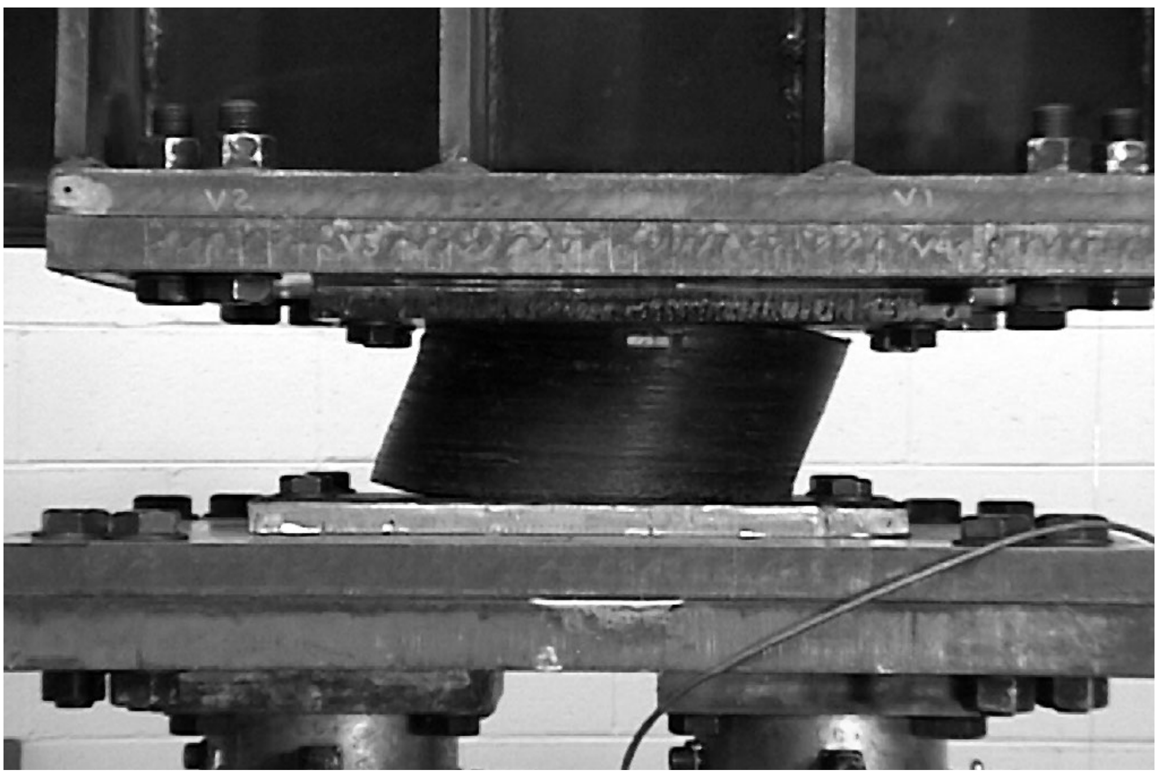

Figure 4.11 Specimen J07 at 50% shear deformation

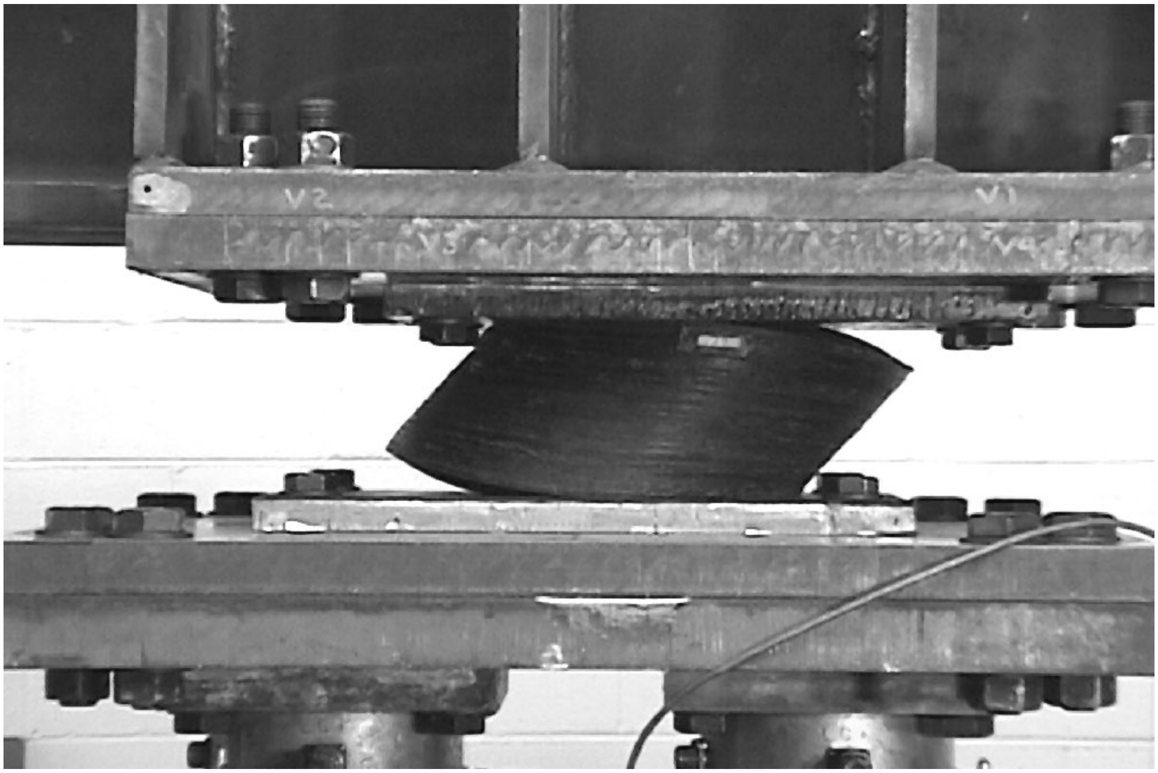

Figure 4.12 Specimen J07 at 100% shear deformation

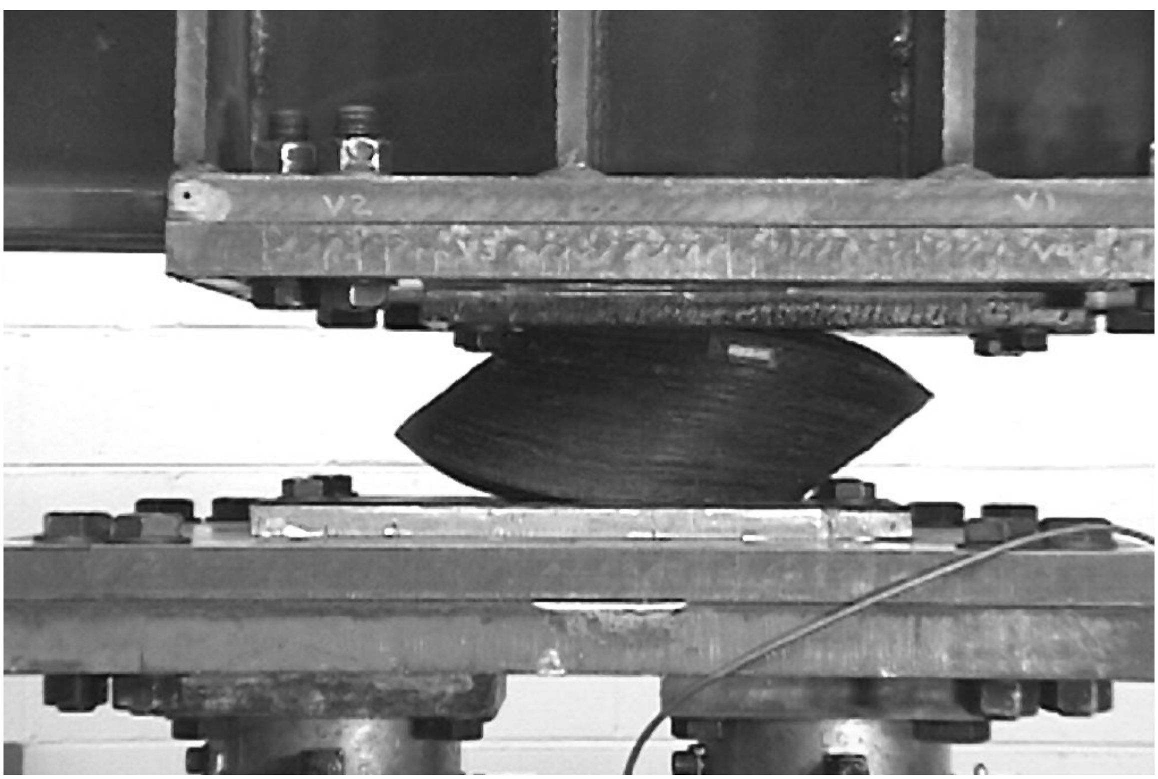

Figure 4.13 Specimen J07 at 150% shear deformation

The results of the vertical test are presented in Figure 4.14. The vertical axis represents the vertical imposed load and the horizontal axis represents the relative displacement between base plates. The dashed straight line corresponds to the average stiffness of the specimen during the cyclic part of testing.

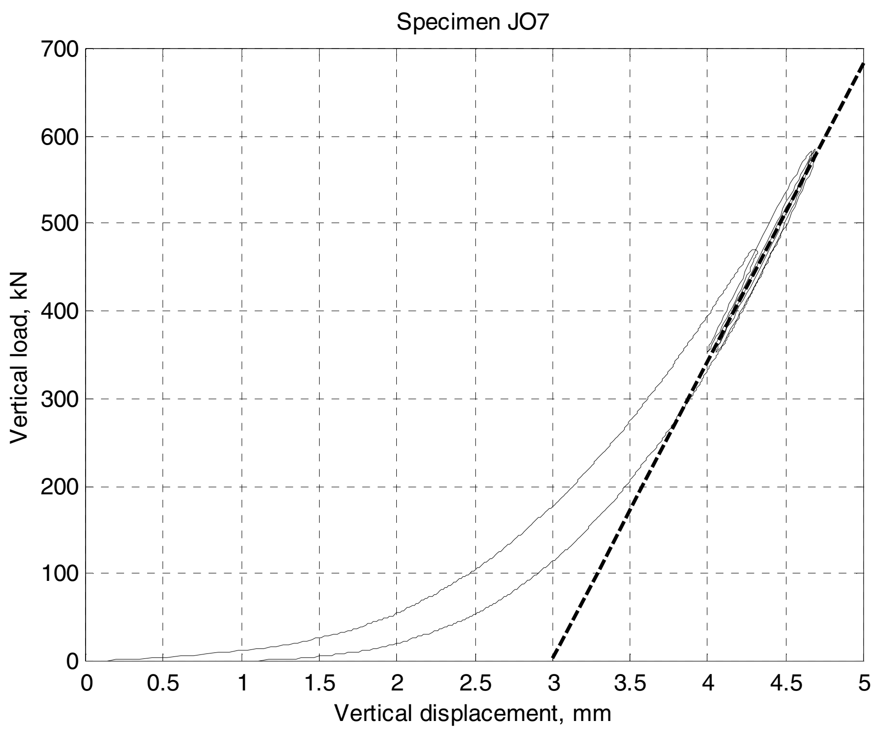

Figure 4.14 Imposed vertical load versus vertical displacement diagram

The bearings were handmade. The top and bottom surfaces were not very flat, and the reinforcement was not taut before loading, causing significant run-in before the bearings began to develop vertical stiffness. The vertical stiffness shows a certain amount of scatter, reflecting the amateurish method of construction, but the average effective modulus, E_c , is 466 MPa, which, with a steel reinforced bearing and a rubber modulus of 0.69 MPa, would mean a shape factor of 10. Clearly, these bearings prove that it is relatively easy to match the vertical stiffness of a typical steel bearing with fiber reinforcement.

The results of the horizontal test are presented in Figures. 4.15 and 4.16. The vertical axis represents the horizontal imposed load, and the horizontal axis represents the horizontal displacement. The dashed straight line corresponds to the horizontal average stiffness of the specimen during the cyclic part of testing. Figure 4.15 shows the horizontal imposed load versus horizontal displacement during the test with the 6.90 MPa initial vertical load. The result of the next test with a 3.45 MPa initial vertical load is presented in Figure 4.16. A short summary of the experimental study on specimen J07 is presented in Tables 4.5a and 4.5b.

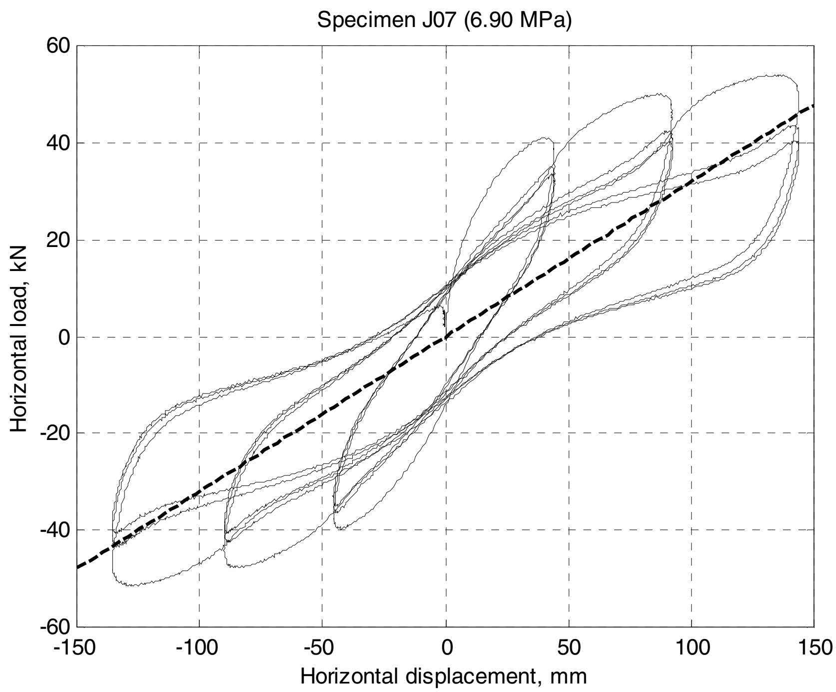

Figure 4.15 Horizontal test result for 6.90 MPa initial vertical pressure

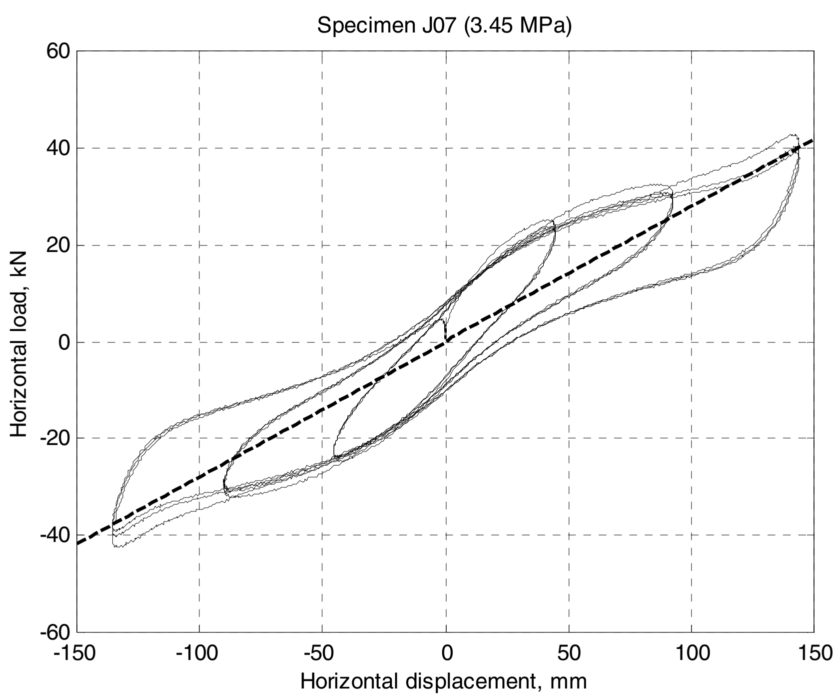

Figure 4.16 Horizontal test result for 3.45 MPa initial vertical pressure

Table 4.5a Vertical test result in the second series

Specimen	Initial vertical pressure MPa	Vertical pressure magnitude MPa	Average vertical stiffness during cyclic reversals kN/m
J07	6.90	1.73	340,375

Table 4.5b Horizontal test results in the second series

Specimen	Vertical pressure MPa	Shear strain magnitude %	Effective stiffness, K^h_{eff} kN/m	Average stiffness, K^h_{av} kN/m	Equivalent damping*, ξ %
J07	3.45	50[1)]	552	510	14.7
J07	3.45	100[2)]	353	327	14.2
J07	3.45	150[3)]	304	256	12.8
J07	3.45	50, 100, 150[4)]	304	278	7.6
J07	6.90	50[1)]	896	752	14.2
J07	6.90	100[2)]	536	427	13.5
J07	6.90	150[3)]	377	273	13.9
J07	6.90	50, 100, 150[4)]	377	319	8.6

(1) Three cycles with 50% shear deformation magnitude were chosen to calculate these parameters.
(2) Three cycles with 100% shear deformation magnitude were chosen to calculate these parameters.
(3) Three cycles with 150% shear deformation magnitude were chosen to calculate these parameters.
(4) Data from all nine cycles were used to calculate these parameters.

A seismic isolator must provide a very high vertical stiffness and a low horizontal one. The behavior of the fiber-reinforced bearing satisfies these demands: the shear horizontal stiffness is more than 1000 times less than the vertical one. The specimen behavior during the test clearly proves that it is relatively easy to match the shear stiffness of a typical steel bearing with fiber reinforcement.

The other distinguishing property of the specimen is a difference in the energy dissipation for various vertical pre-loads, which can be seen by comparing Figures 4.15 and 4.16 and from results presented in Table 4.5b. In both figures there is a distinct thickening of the hysteresis loop that is caused by an increase in the equivalent viscous damping ratio, as shown in Table 4.5b. This has been observed in many other test programs on elastomeric steel-reinforced bearings, e.g., (Kelly 1991; Taniwangsa, Clark, and Kelly 1995), where an increase in pressure produces an increase in damping.

4.4 Discussion of the Experimental Results

The results of these tests indicate that the flexibility of the fiber reinforcement has only a small effect on the shear stiffness of a bearing. The stiffness is reduced to around 80–85% of that of the steel-reinforced bearing of the same size and thickness of the elastomer.

An unexpected factor, however, is the level of damping shown by the fiber-reinforced bearings. The compound used in these bearings is an early example of a high-damping bearing with an equivalent viscous damping of around 8% at 100% shear strain. In the tests the damping is around 18% at 50% shear, 15% at 100% shear, and from 13% to 15% at 150% shear, implying that the energy dissipation of the composite bearings significantly exceeds that of the rubber compound. A possible explanation for this effect is that each individual fiber of a single plane of reinforcement is made up of an extremely large number of single fibers twisted into a thread. The modulus of elasticity of the fiber material is extremely high, on the order of 120,000 MPa, and the possibility of extending or compressing fibers at the outer edges of a thread is extremely unlikely. Therefore, the flexure of the thread is likely caused by an interfacial slip of one fiber over another. The tension on the thread, induced by the vertical load through the lateral bulging of the rubber, causes an interfacial shear stress between the fibers in a single thread. This frictional stress must be overcome before the threads can bend to accommodate the warping of the cross section.

Clearly more experimental work is needed to verify this hypothesis and to determine the various parameters that influence energy dissipation. The concept is very promising because currently it is difficult to incorporate high levels of intrinsic damping into natural rubber compounds by conventional means (i.e., adding carbon, oils, or resins) without degrading some of the advantageous properties of the elastomer. For isolators to be used for small buildings in highly seismic environments where the isolators are lightly loaded, it is advantageous to use an elastomer with a very low shear modulus 0.3–0.4 MPa, but such a compound will have low damping. If the fiber reinforcement can add significant damping (in the range of 13–18%, which is all that is needed in an isolation system

(Kelly 1999)) then even lower modulus elastomers could be used. The possibility then exists for using continuous strip isolators to isolate multi-story masonry wall buildings.

The incentives for using fiber-reinforced isolators are twofold: (1) they are much lighter than steel-reinforced isolators and (2) they could be less costly, if made by a mass production manufacturing process like tires. However, if bonding to steel end plates is required, these advantages would be considerably lessened due to the cost and weight of the steel end plates and the need for a more elaborate bonding process.

The test results show that it is possible to use unbonded isolators. Although a considerable amount of edge uplift occurs, the force-displacement curve always has positive stiffness, indicating that the bearing is still stable at 150% shear deformation even though it appears to be rolling. These test bearings were circular and are more susceptible to rollout than a long strip isolator would be. The goal of this research is to promote the use of long strip isolators.

Long strip isolators would be more stable than circular isolators and their stiffness less sensitive to vertical load. It will be necessary to have strip isolators made and tested for both in longitudinal and lateral displacements to verify that a stable and effective isolation system is feasible.

5 Concluding Remarks

Both the analytical and experimental work demonstrate that for the seismic protection of buildings it is possible to replace the steel reinforcement currently used in isolators with fiber reinforcement. The resulting isolator is certainly much lighter than the steel-reinforced bearing. Further studies must address the manufacturing process and whether the process of assembling and vulcanizing the isolator can be streamlined. Whether strip isolators can be produced at a much reduced cost must also be assessed.

If these issues are successfully addressed, then seismic isolation can be extended to developing countries where the housing, schools, and other public buildings are not seismically safe. It can be argued that the technology to build isolators is not available in these countries. The process envisaged for manufacturing strip isolators in such countries is very similar to the manufacturing process for tires. There are many highly seismic countries, for example, India and Iran, where the rural population live and work in unsafe buildings. Both India and Iran have very highly developed tire industries.

An enormous amount of research funding has been spent over the past ten years on attempting to develop and implement active control techniques for the seismic protection of buildings, and several buildings using active control systems have been built in Japan. There have also been proposals to develop smart isolators and intelligent isolation systems. The value of this research endeavor is questionable. It is unlikely to prove practical even for large, expensive structures and will definitely never be of any use in developing countries. On the other hand, development of lightweight, cost-effective isolators is crucial if this method of seismic protection is to be applied to a wide range of buildings, such as public housing, schools, and medical centers, in earthquake-prone areas of the world.

REFERENCES

Clough, R. W., and Penzien, J. 1975. *Dynamics of Structures*. New York: McGraw-Hill.

Gent, A. N., and Meinecke, E. A. 1970. Compression, Bending and Shear of Bonded Rubber Blocks. *Polymer Engineering and Science* 10(1):48–53.

Gent, A. N., and Lindley, P. B. 1959. Compression of Bonded Rubber Blocks. *Proceedings,* Institution of Mechanical Engineers 173(3):111–22.

Kelly, J. M. The Role of Damping in Seismic Isolation. 1999. *J. Earthquake Engineering and Structural Dynamics* 28(1):3–20.

Kelly, J. M. *Dynamic and Failure Characteristics of Bridgestone Isolation Bearings.* 1991. Report UCB/EERC-91/04. Berkeley, Calif.: University of California.

Rocard, Y. 1937. Note sur le Calcul des Propriétés Élastique des Supports en Caotchouc Adhérent. *J. Physique et de Radium* 8:197.

Taniwangsa, W., Clark P., and Kelly J. M. 1995. *Natural Rubber Isolation Systems for Earthquake Protection of Low-Cost Buildings*. Report UCB/EERC-95/12. Berkeley, Calif.: University of California.

Timoshenko, S. P., and Goodier, J. N. 1970. *Theory of Elasticity.* 3rd ed. New York: McGraw-Hill.